

JAERI-M

8 0 4 2

A NUMERICAL CODE SELENE TO CALCULATE  
AXISYMMETRIC TOROIDAL MHD EQUILIBRIA

January 1979

Tatsuoki TAKEEDA and Toshihide TSUNEMATSU

日本原子力研究所  
Japan Atomic Energy Research Institute

この報告書は、日本原子力研究所が JAERI-M レポートとして、不定期に刊行している研究報告書です。入手、複製などのお問い合わせは、日本原子力研究所技術情報部（茨城県那珂郡東海村）あて、お申しこしください。

JAERI-M reports, issued irregularly, describe the results of research works carried out in JAERI. Inquiries about the availability of reports and their reproduction should be addressed to Division of Technical Information, Japan Atomic Energy Research Institute, Tokai-mura, Naka-gun, Ibaraki-ken, Japan.

A Numerical Code SELENE To Calculate  
Axisymmetric Toroidal MHD Equilibria

Tatsuoki TAKEDA and Toshihide TSUNEMATSU  
Division of Thermonuclear Fusion Research,  
Tokai Research Establishment, JAERI

(Received December 15, 1978)

A new algorithm to calculate an MHD equilibrium of axisymmetric toroidal plasmas has been devised and applied successfully to the case of a fixed boundary nonlinear eigenvalue problem. The algorithm is based on a combination of a usual finite element method and a new iteration scheme whereby the mesh structure for calculation is corrected for the finite elements always to be along magnetic surfaces. Very high accuracy is thus attained in the vicinity of the magnetic axis and in the regions where magnetic surfaces are closely located.

Keywords: MHD equilibrium, Finite element method, Axisymmetric toroidal plasma, Tokamak plasma, Computer code

JAERI-M 8042

軸対称トーラス・プラズマのMHD平衡計算コード  
(SELENE)

日本原子力研究所東海研究所核融合研究部  
竹田 辰興・常松 俊秀

(1978年12月15日受理)

軸対称トーラス・プラズマのMHD平衡の計算をする為の新しい方法を考案し、固定境界非線形固有値問題として扱われる場合に適用して満足すべき結果を得た。この方法は有限要素法と新しい逐次近似法に基づくものである。逐次近似の過程では、有限要素が常に磁気面に沿って並ぶようにメッシュ構造が補正されつつ計算が進行する。この結果、磁気軸近傍および磁気面の混んでいる付近で高い計算精度が達成される。

## 目 次

1.	はじめに.....	1
2.	計算法.....	2
2.1	有限要素法による定式化.....	2
2.2	逐次近似法.....	6
2.3	結果のスケールリング.....	7
2.4	表面積分量と局部安定条件.....	8
3.	計算結果.....	11
4.	まとめおよび討論.....	12
付 録	-----	53
A 1.	メイン・プログラムとCOMMON変数.....	54
A 2.	JOB制御文.....	59
A 3.	入力データ.....	60
A 4.	ライン・プリンター出力例.....	63

Contents

1.	Introduction.....	1
2.	Method of Calculation.....	2
2.1	Numerical formulation of the problem by the finite element method..	2
2.2	Iteration schemes.....	6
2.3	Scaling of the results.....	7
2.4	Surface integrals and local stability criterion.....	8
3.	Results of Calculation.....	11
4.	Summary and Discussions.....	12
Appendix -----		53
A1.	The main program and COMMON variables.....	54
A2.	Job control statement.....	59
A3.	Input data format.....	60
A4.	An example of line printer output.....	63

## 1. Introduction

It is required to develop numerical codes by which one can calculate MHD equilibria of a toroidal plasma accurately at high speed. This requirement comes from the fact that recently numerical codes for MHD equilibrium calculation are incorporated with codes which calculate two-dimensional transports in a tokamak plasma<sup>1-3)</sup> and multidimensional MHD stability analyses<sup>4,5)</sup>. As for the former, the equilibrium is calculated a hundred times to a thousand times during an analysis. In the latter the overall accuracy of stability analysis is usually limited by accuracy of the equilibrium calculation. It is necessary to calculate equilibrium near a magnetic axis very accurately because conventional numerical codes for equilibrium calculation are formulated on the basis of square meshes in an  $r$ - $z$  poloidal plane but stability calculation is carried out on square meshes in  $\psi$ - $\chi$  plane.

A successful example of equilibrium code in which a system of meshes are constructed with respect to the magnetic surface is that based on the waterbag method by Potter et al.<sup>6)</sup> In this method pressure balance is satisfied on a finite number of magnetic surfaces and during iterations residual forces push the magnetic surfaces to equilibrium configuration. Takeda applied similar method<sup>7)</sup> to write a numerical code in which a functional of the finite element method made of Grad-Shafranov equation is directly minimized by using a nonlinear programming algorithm. This method is not very successful as for the accuracy and CPU time required for the calculation, because nonlinear programming algorithms are too general and not efficient as compared with other specific iteration schemes.

We developed a new equilibrium code in which the structure of meshes are corrected during iterations so that the  $\psi$  value of a certain mesh is always same and the magnetic axis is always on a mesh point. The algorithm is, in principle, the usual solution method of a partial differential equation by the finite element method.

In the next section we describe the method of calculation. We show some examples of results of calculations and also examine the accuracy by calculation of the surface integrals and local stability criterion in Section 3. Section 4 summarizes and discusses the algorithm.

## 2. Method of Calculation

An equation to be solved is the Grad-Shafranov's equilibrium equation<sup>8)</sup>;

$$\Delta^* \psi = \frac{\partial^2 \psi}{\partial r^2} - \frac{1}{r} \frac{\partial \psi}{\partial r} + \frac{\partial^2 \psi}{\partial z^2} = -\mu_0 r j_\phi, \quad (1)$$

$$j_\phi = -r \frac{dp}{d\psi} + \frac{1}{\mu_0 r} \frac{dT}{d\psi}, \quad (2)$$

where  $p$  and  $T$  are plasma pressure and toroidal field functions, respectively, and both are functions of the poloidal flux function  $\psi$ .

## 2.1 Numerical formulation of the problem by the finite element method

As we are mainly interested in the development of a high accuracy and high speed MHD equilibrium code we restrict ourselves to a fixed boundary solution as a nonlinear eigenvalue problem. Therefore, the equation is rewritten as<sup>8)</sup>

$$\Delta^* \psi = -\lambda \mu_0 r j_{\phi_0}, \quad (3)$$

$$\lambda j_{\phi_0} = j_\phi, \quad (4)$$

The functional form of the toroidal current density  $j_{\phi_0}$  is given before calculation. The eigenvalue ( $\lambda$ ) and eigenvector ( $\psi$ ) are calculated under the boundary conditions;

$$\psi = 0 \quad \text{at the plasma boundary,} \quad (5)$$

$$\psi = -1 \quad \text{at the magnetic axis.} \quad (6)$$

Practical constraints such as magnitude of total toroidal current are imposed by using an appropriate scaling law after a solution is obtained (see 2.3). To obtain the solution of the above problem, iterations are performed as follows,

$$\Delta^* \psi^{n+1} = -\lambda^n r j_{\phi_0} \left( \frac{\psi^n}{\psi_0^n} \right), \quad (7)$$

$$\lambda^{n+1} = - \frac{1}{\psi_0^{n+1}} \lambda^n, \quad (8)$$

where  $\psi^{n+1}$  is the (n+1)th step's  $\psi$ -value at the magnetic axis. The iteration



is terminated by using a stopping parameter  $\epsilon$  as

$$\left| \frac{-1}{\psi_0^{n+1}} - 1 \right| \leq \epsilon . \quad (9)$$

Solution of eq.(7) is the usual one based on the finite element method where the object function is derived as a weak form of the equation<sup>9)</sup>,

$$L(\psi^{n+1}) = (\Delta^* \psi^{n+1}, \psi^{n+1}) - 2(f(\psi^n), \psi^{n+1}), \quad (10)$$

$$f(\psi^n) = -\lambda^n \mu_0 r j_{\phi_0} (-\psi^n / \psi_0^n), \quad (11)$$

where  $(u,v)$  denotes a scalar product of functions  $u$  and  $v$  as

$$(u,v) = \int dS u \cdot v. \quad (12)$$

In our problem the functional  $L$  is derived in a poloidal plane of the axisymmetric torus as

$$L(\psi^{n+1}) = -\int r dr dz \left\{ \left( \frac{1}{r} \frac{\partial \psi^{n+1}}{\partial r} \right)^2 + \left( \frac{\partial \psi^{n+1}}{\partial z} \right)^2 - \frac{2\lambda^n}{r} j_{\phi_0} \left( \frac{\psi^n}{\psi_0^n} \right) \psi^{n+1} \right\}. \quad (13)$$

By using an appropriate set of basis functions, the functional  $L$  (eq.(13)) is represented by  $N$  parameters  $(\psi_1^{n+1}, \psi_2^{n+1}, \dots, \psi_N^{n+1})$  where  $N$  is the number of the node points inside the boundary in the upper half plane (Fig.1).

Simultaneous linear equations with respect to  $\psi_i^{n+1}$  is immediately derived from eq.(13), that is,

$$A \Psi^{n+1} = B^n, \quad (14)$$

where  $t_{\Psi}^{n+1} = (\psi_1^{n+1}, \psi_2^{n+1}, \dots, \psi_N^{n+1}), \quad (15)$

$$B^n \cdot \Psi^{n+1} = -2(f(\psi^n), \psi^{n+1}). \quad (16)$$

Thus the solution for the  $(n+1)$ -th iteration is obtained. The matrix  $A$  is derived as follows. In the finite element method the integral in eq.(13) is represented by a sum of integrals for all the elements,

$$L = \sum_{elm} L_{elm}. \quad (17)$$

An integral for an element ( $L_{elm}$ ) is represented by an integral of a quadratic form of  $\psi$ ,  $\partial\psi/\partial r$ ,  $\partial\psi/\partial z$  with respect to a matrix F as

$$L_{elm} = \int_{elm} (\psi, \frac{\partial\psi}{\partial r}, \frac{\partial\psi}{\partial z}) F \begin{pmatrix} \psi \\ \frac{\partial\psi}{\partial r} \\ \frac{\partial\psi}{\partial z} \end{pmatrix} dS, \quad (18)$$

where  $F = \begin{pmatrix} 0, & 0, & 0 \\ 0, & 1/r, & 0 \\ 0, & 0, & 1/r \end{pmatrix}$ . (19)

In our case (Fig.1), all elements except for the innermost layer elements are rectangular and the meshes in the innermost layer are triangular. For the rectangular meshes the following isoparametric transformation is effective to obtain a continuous solution<sup>9)</sup>. First we transform an arbitrary shaped rectangular mesh in r-z plane into a regular square mesh in  $\xi$ - $\eta$  plane (Fig.2). The transformation is represented by a bilinear forms of  $\xi$  and  $\eta$  as

$$r = a_0 + a_1\xi + a_2\eta + a_3\xi\eta, \quad (20)$$

$$z = b_0 + b_1\xi + b_2\eta + b_3\xi\eta, \quad (21)$$

where  $a_i$  and  $b_i$  are functions of r, z coordinates of the node points of the rectangle. Then we represent the  $\psi$ -values in the element by a bilinear form of  $\xi$  and  $\eta$ , that is,

$$\psi = (1, \xi, \eta, \xi\eta) S \begin{pmatrix} \psi_i \\ \psi_j \\ \psi_k \\ \psi_l \end{pmatrix}, \quad (22)$$

where  $S = \begin{pmatrix} \alpha_i & \alpha_j & \alpha_k & \alpha_l \\ \beta_i & \beta_j & \beta_k & \beta_l \\ \gamma_i & \gamma_j & \gamma_k & \gamma_l \\ \delta_i & \delta_j & \delta_k & \delta_l \end{pmatrix}$ , (23)

$$\alpha_i = [\xi_j\eta_j(\xi_k\eta_l - \xi_l\eta_k) + \xi_k\eta_k(\xi_l\eta_j - \xi_j\eta_l) + \xi_l\eta_l(\xi_j\eta_k - \xi_k\eta_j)]/D_{ijkl}, \quad (24)$$

$$\begin{aligned}
 D_{ijkl} = & \xi_i \xi_j [\eta_j (\xi_k - \xi_\ell) + \eta_k (\xi_\ell - \xi_j) + \eta_\ell (\xi_j - \xi_k)] \\
 & - \xi_j \xi_k [\eta_k (\xi_\ell - \xi_i) + \eta_\ell (\xi_i - \xi_k) + \eta_i (\xi_k - \xi_\ell)] \\
 & + \xi_k \xi_\ell [\eta_\ell (\xi_i - \xi_j) + \eta_i (\xi_j - \xi_\ell) + \eta_j (\xi_\ell - \xi_i)] \\
 & - \xi_\ell \xi_i [\eta_i (\xi_j - \xi_k) + \eta_j (\xi_k - \xi_i) + \eta_k (\xi_i - \xi_j)] , \quad (25)
 \end{aligned}$$

$$\beta_i = [\eta_j \eta_k (\xi_j - \xi_k) + \eta_k \eta_\ell (\xi_k - \xi_\ell) + \eta_\ell \eta_j (\xi_\ell - \xi_j)] / D_{ijkl} , \quad (26)$$

$$\gamma_i = [\xi_j \xi_k (\eta_j - \eta_k) + \xi_k \xi_\ell (\eta_k - \eta_\ell) + \xi_\ell \xi_j (\eta_\ell - \eta_j)] / D_{ijkl} , \quad (27)$$

$$\delta_i = [\xi_j (\eta_\ell - \eta_k) + \xi_k (\eta_j - \eta_\ell) + \xi_\ell (\eta_k - \eta_j)] / D_{ijkl} . \quad (28)$$

Equations for j, k, and ℓ nodes are obtained by changing the suffixes cyclically in the order of i, j, k, and ℓ. In the triangular elements the following equations are applied,

$$D_{ijk} = \xi_i (\eta_j - \eta_k) + \xi_j (\eta_k - \eta_i) + \xi_k (\eta_i - \eta_j) , \quad (29)$$

$$\alpha_i = (\xi_j \eta_k - \xi_k \eta_j) / D_{ijk} , \quad (30)$$

$$\beta_i = (\eta_j - \eta_k) / D_{ijk} , \quad (31)$$

$$\gamma_i = (\xi_j - \xi_k) / D_{ijk} . \quad (32)$$

Numerical values for the above representation is easily derived in our case and the matrix S is obtained as

$$\underline{S} = \begin{pmatrix} 1 & 0 & 0 & 0 \\ -1 & 0 & 0 & 1 \\ -1 & 1 & 0 & 0 \\ 1 & -1 & 1 & -1 \end{pmatrix} , \quad \text{rectangular case,} \quad (33)$$

$$\underline{S} = \begin{pmatrix} 1/3 & 1/3 & 1/3 \\ 2/3 & -1/3 & -1/3 \\ 0 & -1/\sqrt{3} & 1/\sqrt{3} \end{pmatrix} , \quad \text{triangular case,} \quad (34)$$

Thus we obtain a set of values for  $\psi$ ,  $\partial\psi/\partial\xi$ ,  $\partial\psi/\partial\eta$  for an arbitrary point in an element as

$$\begin{pmatrix} \psi \\ \partial\psi/\partial\xi \\ \partial\psi/\partial\eta \end{pmatrix} = \begin{pmatrix} 1 & \xi & \eta & \xi\eta \\ 0 & 1 & 0 & \eta \\ 0 & 0 & 1 & \xi \end{pmatrix} \underline{S} \begin{pmatrix} \psi_i \\ \psi_j \\ \psi_k \\ \psi_l \end{pmatrix}, \quad (35)$$

To evaluate the integral for each element ( $L_{elm}$ ) we should calculate the coefficient matrix  $\underline{T}$  for the transformation ( $\partial\psi/\partial\xi, \partial\psi/\partial\eta \rightarrow \partial\psi/\partial r, \partial\psi/\partial z$ ),

$$\begin{pmatrix} \psi \\ \partial\psi/\partial r \\ \partial\psi/\partial z \end{pmatrix} = \underline{T} \begin{pmatrix} \psi \\ \partial\psi/\partial\xi \\ \partial\psi/\partial\eta \end{pmatrix}, \quad (36)$$

where

$$\underline{T} = \begin{pmatrix} 1 & 0 & 0 \\ 0 & b_2 + b_3\xi & -b_1 - b_3\eta \\ 0 & -a_2 - a_3\xi & a_1 + a_3\eta \end{pmatrix} \frac{1}{J}, \quad (37)$$

$$\text{where } J = (a_1 + a_3\eta)(b_2 + b_3\xi) - (a_2 + a_3\xi)(b_1 + b_3\eta). \quad (38)$$

By the above procedure we obtain a quadratic form of  $\psi_i, \psi_j, \psi_k$ , and  $\psi_l$  for the functional  $L_{elm}$ . From the quadratic form corresponding to  $L$  (eq.(17)) the matrix  $A$  is derived.

## 2.2 Iteration schemes

There are two kinds of iteration process in this algorithm, one is the inner iteration by which the eigenvalue  $\lambda$  is converged, and the other is the outer iteration by which the mesh structure is converged. The most important feature of this algorithm is that the positions of the node points are corrected every outer iteration so that the elements are defined along the magnetic surfaces. The advantages of the algorithm are evident, that is, the accuracy of the calculation near the magnetic axis is extremely good as compared with the usual methods and that of outside of the magnetic axis is also very good even when we treat a high beta toroidal equilibrium.

This algorithm is similar to that of the waterbag method by Potter et al. in that the mesh points are traced every iteration. The waterbag method is, however, principally the Lagrangian calculation and ours is the sequence of the Eulerian calculation for a system of variable meshes. The disadvantage of the former algorithm that the position of the magnetic axis is

difficult to calculate accurately is easily overcome by our method.

The overall iteration procedure is summarized as follows,

- (1) Prepare initial meshes.
- (2) Solve the equation for  $\psi^{n+1}$ ,

$$\psi^{n+1} = \Delta^{*-1} \lambda^n f(\psi^n, r). \quad (39)$$

- (3) Normalize the  $\psi$  values by the value at the magnetic axis and obtain the (n+1)-th eigenvalue  $\lambda^{n+1}$ ,

$$\lambda^{n+1} = \frac{1}{\psi_0^{n+1}} \lambda^n. \quad (40)$$

- (4) If  $|\psi_0^{n+1} - 1|$  is not sufficiently small then return to the process (2).
- (5) Calculate equi- $\psi$  surfaces and reconstruct meshes.
- (6) If  $|r_{\text{axis}}^{m+1} - r_{\text{axis}}^m|$  is not sufficiently small then return to the process (2), where m is the number of the outer iteration.
- (7) End of iterations.

The flowchart and program structure are shown in Fig.3.

### 2.3 Scaling of the results

In our calculation the range of the variable  $\psi$  is restricted within  $[-1.0, 0.0]$ . Therefore, it is necessary to transform the variable if the physical quantities such as the total plasma current, maximum pressure and so on are to be adjusted to given values. For this purpose the scaling of equilibrium is often used<sup>5,10)</sup> When an equilibrium is transformed into a new equilibrium, the new equilibrium quantities  $\hat{X}$ 's are derived using scaling factor  $\sigma$  and the old quantities  $X$ 's as

$$\hat{\psi} = \sigma \psi, \quad (41)$$

$$\hat{B}_p = \sigma B_p, \quad (42)$$

$$\hat{j}_\phi = \sigma j_\phi, \quad (43)$$

$$\hat{p} = \sigma^2 p, \quad (44)$$

$$\left( T \frac{dT}{d\psi} \right) = \sigma T \frac{dT}{d\psi}, \quad (45)$$

$$\hat{T}^2 = T_a^2 + \sigma^2 (T^2 - T_a^2), \quad (46)$$

$$\hat{q}^2 = q^2 \frac{\hat{T}^2}{T^2 \sigma^2}, \quad (47)$$

If the prescribed total plasma current is  $I_p$  the scaling factor  $\sigma$  is chosen as

$$\sigma = \frac{I_p}{\lambda \int j_{\phi_0} dS}. \quad (48)$$

It is needless to say that, by the scaling, the functional dependences of  $p$  and  $T$  on  $\Phi$  are changed from the given ones. In some cases this causes serious problems. But in the cases such as the optimization of the MHD equilibrium with respect to the beta values or two-dimensional transport calculation this is not a very important restriction. Therefore we use the above scaling procedure in our code.

#### 2.4 Surface integrals and local stability criterion

When we apply the results of the equilibrium calculations to the stability and transport analyses, we should calculate magnetic field and many kinds of surface integrals with high accuracy. For convenience of the numerical calculation, these quantities are classified into 5 groups as (1) Quantities which are derived directly from the equilibrium calculations by the finite element method.

In our numerical program these quantities are evaluated at the center of each element.

$$\psi, \frac{\partial \psi}{\partial r}, \frac{\partial \psi}{\partial z}, r, z, d\ell, T^2, p, j_{\phi}, s,$$

where  $d\ell$  is the line length across an element along the magnetic surface and  $s$  is the area of the element.

(2) Surface integrals defined as functions of the magnetic surface.

1. Safety factor:  $q$

$$q = \frac{1}{2\pi} \oint \frac{T}{r^2 B_p} d\ell, \quad (49)$$

2. Other surface quantities which are derived directly from the quantities in the group (1).

$$C_1 = \oint \frac{d\ell}{B_p^3 r^2}, \quad (50)$$

$$C_2 = \oint \frac{d\ell}{B_p^3 r^4}, \quad (51)$$

$$C_3 = \oint \frac{d\ell}{B_p^3}, \quad (52)$$

$$C_4 = \oint \frac{r^2 d\ell}{B_p}, \quad (53)$$

$$C_5 = \oint B_p d\ell, \quad (54)$$

$$C_6 = \oint B_p r^2 d\ell, \quad (55)$$

$$V = \int dV, \quad (56)$$

$$\frac{dV}{d\psi} = 2\pi \oint \frac{d\ell}{B_p}, \quad (57)$$

$$\frac{dU}{d\psi} = 2\pi \oint \frac{d\ell}{B_p r^2}, \quad (58)$$

these quantities are also used for the calculation of the Mercier criterion.

(3) Poloidal coordinate.

$$\chi = \frac{1}{q(\psi)} \int \frac{T d\ell}{B_p r^2}. \quad (59)$$

(4) Volume integrals necessary to evaluate beta values.<sup>5)</sup>

$$I_{pr} = \iiint J d\psi d\chi p, \quad (60)$$

$$I_{pr^2} = \iint J d\psi d\chi p^2, \quad (61)$$

$$I_{B^2} = \iint J d\psi d\chi \left( B_p^2 + \frac{T^2}{r^2} \right), \quad (62)$$

$$I_V = \iint J d\psi d\chi, \quad (63)$$

$$I_I = \iint J d\psi d\chi j_\phi. \quad (64)$$

By using these quantities, the usual beta value( $\beta$ ), the poloidal beta value( $\beta_p$ ) and the reactor plasma beta value( $\beta^*$ ) are given as

$$\beta = 2 \frac{I_{pr}}{I_{B^2}}, \quad (65)$$

$$\beta_p = \frac{8\pi}{\mu_0} \frac{I_{pr}}{I_I^2}, \quad (66)$$

$$\beta^* = 2 \frac{I_{pr}^2 I_V}{I_{B^2}}, \quad (67)$$

(5) Quantities obtained from derivatives of the above quantities with respect to  $\psi$ .

Magnetic shear  $S$  (Eq.68) and  $\psi$  derivative of pressure belong to this class.

$$S = - \frac{\frac{d}{d\psi} \left[ T \int \left( \frac{1}{r^2 B_p} \right) d\ell \right]}{\left( \frac{dV}{d\psi} \right)^3}. \quad (68)$$

These quantities are transferred to the stability analyses codes and transport analyses codes. The mercier criterion is evaluated in our equilibrium code. The plasma is stable against a local instability if

$$M = M_0 + M_1 + M_2 > 0, \quad (69)$$

for all  $\psi$  values, where

$$M_0 = \frac{1}{4} S^2, \quad (70)$$



$$M_1 = \mu \frac{dp}{od\psi} \left[ c_1 \frac{T S}{\left(\frac{dV}{d\psi}\right)^3} + \left( c_2 T^2 + \frac{dU}{d\psi} \right) \frac{\left(\frac{d^2V}{d\psi^2}\right)}{\left(\frac{dV}{d\psi}\right)^6} \right], \quad (71)$$

$$M_2 = -\mu_0^2 \left(\frac{dp}{d\psi}\right)^2 \left[ T^2 (c_2 c_3 - c_1^2) + c_3 \frac{dU}{d\psi} \right] \frac{1}{\left(\frac{dV}{d\psi}\right)^6}, \quad (72)$$

### 3. Results of Calculation

One of the main purpose of development of this code is to calculate accurately wider class of MHD equilibrium, that is, the functional forms of  $p(\psi)$  and  $T(\psi)$  should be selected arbitrarily as possible. This code can calculate an equilibrium for numerically given distributions of pressure and toroidal field functions, which is very important when we use the code to transport analyses.

In the following, however, we choose the dependences of  $p$  and  $T$  adopted by ORNL group for the convenience of parameter survey<sup>11)</sup>. The pressure of the plasma is expressed by a nonlinear function of  $\psi$  as

$$p = \beta_J p_0' \left\{ (\psi - \psi_b) - \frac{\alpha}{2} [(\psi - \psi_m)^2 - (\psi_b - \psi_m)^2] \right. \\ \left. + \frac{\gamma}{L+1} [(\psi - \psi_m)^{L+1} - (\psi_b - \psi_m)^{L+1}] \right\}, \quad L \geq 4 \quad (73)$$

$$\gamma = - \frac{1 - \alpha(\psi_m - \psi_b)}{(\psi_b - \psi_m)^L}, \quad (74)$$

where  $\psi_b$  and  $\psi_m$  are the  $\psi$  values at the plasma boundary ( $\psi_b=0$ ) and the magnetic axis ( $\psi_m=-1$ ), respectively, and  $\alpha$  is a parameter which determines the width of the current column. The toroidal field function  $T$  is related to the pressure function as

$$TT' = \left( \frac{1}{\beta_J} - 1 \right) p' \frac{1}{\langle r^{-2} \rangle} \sim \left( \frac{1}{\beta_J} - 1 \right) R_\theta^2 p', \quad (75)$$

where  $\beta_J$  is a parameter which is approximately equal to the poloidal beta value. In the following several examples of the results are presented.

$$M_1 = \mu \frac{dp}{\rho d\psi} \left[ c_1 \frac{T S}{\left(\frac{dV}{d\psi}\right)^3} + \left( c_2 T^2 + \frac{dU}{d\psi} \right) \frac{\left(\frac{d^2V}{d\psi^2}\right)}{\left(\frac{dV}{d\psi}\right)^6} \right], \quad (71)$$

$$M_2 = -\mu_0^2 \left(\frac{dp}{d\psi}\right)^2 \left[ T^2 (c_2 c_3 - c_1^2) + c_3 \frac{dU}{d\psi} \right] \frac{1}{\left(\frac{dV}{d\psi}\right)^6}, \quad (72)$$

### 3. Results of Calculation

One of the main purpose of development of this code is to calculate accurately wider class of MHD equilibrium, that is, the functional forms of  $p(\psi)$  and  $T(\psi)$  should be selected arbitrarily as possible. This code can calculate an equilibrium for numerically given distributions of pressure and toroidal field functions, which is very important when we use the code to transport analyses.

In the following, however, we choose the dependences of  $p$  and  $T$  adopted by ORNL group for the convenience of parameter survey<sup>11)</sup>. The pressure of the plasma is expressed by a nonlinear function of  $\psi$  as

$$p = \beta_J p_0' \left\{ (\psi - \psi_b) - \frac{\alpha}{2} [(\psi - \psi_m)^2 - (\psi_b - \psi_m)^2] \right. \\ \left. + \frac{\gamma}{L+1} [(\psi - \psi_m)^{L+1} - (\psi_b - \psi_m)^{L+1}] \right\}, \quad L \geq 4 \quad (73)$$

$$\gamma = - \frac{1 - \alpha(\psi_m - \psi_b)}{(\psi_b - \psi_m)^L}, \quad (74)$$

where  $\psi_b$  and  $\psi_m$  are the  $\psi$  values at the plasma boundary ( $\psi_b=0$ ) and the magnetic axis ( $\psi_m=-1$ ), respectively, and  $\alpha$  is a parameter which determines the width of the current column. The toroidal field function  $T$  is related to the pressure function as

$$TT' = \left( \frac{1}{\beta_J} - 1 \right) p' \frac{1}{\langle r^{-2} \rangle} \sim \left( \frac{1}{\beta_J} - 1 \right) R_\theta^2 p', \quad (75)$$

where  $\beta_J$  is a parameter which is approximately equal to the poloidal beta value. In the following several examples of the results are presented.

## (1) Example 1.

Convergence with respect to the number of the finite elements

Poloidal mesh number (MDIV) and radial mesh number (NDIV) are varied from 10 to 30 (Fig.4). The quadratic convergence is shown by the relation between the eigenvalue  $\lambda$  and the number of the meshes (Fig.5).

## (2) Example 2.

Accuracy of calculation of magnetic shear

One of most stringent checks of the accuracy of the calculation is the comparison between the numerically obtained magnetic shear and analytically obtained one, as it contains several quantities which are derived through differentiation processes. In Fig.6, the numerically obtained shears for several large aspect ratio plasmas are shown with analytically obtained ones for cylindrical plasmas of corresponding pitch length ( $L/a$ ). There are slight differences between the analytical and numerical results, especially, near the magnetic axis.

## (3) Example 3.

High beta equilibria

To show that the algorithm is especially effective for the analyses of a high beta toroidal equilibria, we calculated the equilibria for the cases of  $\beta_J = 1, 2, 3$  (Fig.7). In the case of  $\beta_J = 3$ , the magnetic axis is shifted outward by about 40 % of the minor radius of the plasma and the mesh width outside the axis is as small as 1/3 times that inside the axis. Therefore, in such a case, about ten times as many a number of meshes are required if one calculate the equilibrium by the usual rectangular mesh system with the same accuracy.

## (4) Example 4.

Scaling of the equilibrium

To see the effect of the scaling, we show the changes of the equilibria for the same  $p, T$  functions but different scaling factor in Fig.8.

## 4. Summary and Discussions

A computer code to calculate an MHD equilibrium of an axisymmetric toroidal plasma is written on the basis of a combination of a new iteration scheme and the finite element method. By this algorithm mesh structure for the calculation is corrected every outer iteration so that the finite elements are always aligned along magnetic surfaces. Consequently, very high

## (1) Example 1.

Convergence with respect to the number of the finite elements

Poloidal mesh number (MDIV) and radial mesh number (NDIV) are varied from 10 to 30 (Fig.4). The quadratic convergence is shown by the relation between the eigenvalue  $\lambda$  and the number of the meshes (Fig.5).

## (2) Example 2.

Accuracy of calculation of magnetic shear

One of most stringent checks of the accuracy of the calculation is the comparison between the numerically obtained magnetic shear and analytically obtained one, as it contains several quantities which are derived through differentiation processes. In Fig.6, the numerically obtained shears for several large aspect ratio plasmas are shown with analytically obtained ones for cylindrical plasmas of corresponding pitch length ( $L/a$ ). There are slight differences between the analytical and numerical results, especially, near the magnetic axis.

## (3) Example 3.

High beta equilibria

To show that the algorithm is especially effective for the analyses of a high beta toroidal equilibria, we calculated the equilibria for the cases of  $\beta_J = 1, 2, 3$  (Fig.7). In the case of  $\beta_J = 3$ , the magnetic axis is shifted outward by about 40 % of the minor radius of the plasma and the mesh width outside the axis is as small as 1/3 times that inside the axis. Therefore, in such a case, about ten times as many a number of meshes are required if one calculate the equilibrium by the usual rectangular mesh system with the same accuracy.

## (4) Example 4.

Scaling of the equilibrium

To see the effect of the scaling, we show the changes of the equilibria for the same  $p, T$  functions but different scaling factor in Fig.8.

## 4. Summary and Discussions

A computer code to calculate an MHD equilibrium of an axisymmetric toroidal plasma is written on the basis of a combination of a new iteration scheme and the finite element method. By this algorithm mesh structure for the calculation is corrected every outer iteration so that the finite elements are always aligned along magnetic surfaces. Consequently, very high

accuracy is realized near the magnetic axis and regions where magnetic surfaces are located closely. For example, in the case of the MHD stability analyses by the ERATO code<sup>5)</sup> it is expected that the necessary number of meshes for equilibrium calculations ( $N_\psi = N_\chi = N$ ) is about  $N \times N$  (our code) as compared with  $N_r \times N_z \sim 6N \times 3N$  (usual codes). High accuracy of the calculation is demonstrated by several examples, especially, by the calculations of surface integrals.

The present numerical code is applicable only for a fixed boundary nonlinear eigenvalue problem as shown in the previous sections. However, practically, numerical codes for a free boundary plasma or for an FCT equilibrium<sup>12)</sup> are required. Extension of our code to these problems is not essentially difficult.

#### Acknowledgments

The authors would like to thank Dr. M. Tanaka for his valuable discussions. They are also very grateful to Drs. S. Mori and Y. Obata for their continuing encouragements.

References

- 1) Hogan, J.T., "The accessibility of high beta tokamak states", ORNL/TM-6049 May, 1978.
- 2) Byrne, R.N. and Klein, H.H., J. Computational Phys. 26 352 (1978).
- 3) Helton, F.J., Miller, R.L., and Rawls, J.M., J. Computational Phys. 24 117 (1977).
- 4) Grimm, R.C., Greene, J.M., and Johnson, J.L., "Computation of the Magnetohydrodynamic Spectrum in Axisymmetric Toroidal Confinement Systems" in *Methods in Computational Physics* (Academic Press Inc., N.Y., 1976) Vol. 16 p.253.
- 5) Gruber, R., "ERATO stability code" to be published in Computer Physics Communications.
- 6) Potter, D., "Waterbag Methods in Magnetohydrodynamics" in *Methods in Computational Physics* (Academic Press Inc., N.Y., 1976) Vol.16 p.43.
- 7) Takeda, T., "Application of nonlinear optimization to solution of differential and integral equations", IPP 6/147 F3 (1976).
- 8) Lackner, K., Computer Physics Communications 12 33 (1976).
- 9) Strang, G. and Fix, G.J., *An Analysis of the Finite Element Method* (Prentice-Hall, Inc., N.J., 1973).
- 10) Bateman, G. and Peng, Y.-K.M., Phys. Rev. Letters 38 829 (1977).
- 11) Peng, Y.-K.M., Dory, R.A., Nelson, D.B., and Sayer, R.O., Phys. Fluids 21 467 (1978).
- 12) Clarke, J.F. and Sigmar, D.J., Phys. Rev. Letters 38 70 (1977).

## Figure captions

- Fig.1 An example of mesh structure for equilibrium calculation.
- Fig.2 Isoparametric transformation.  
(a) A triangular mesh  
(b) A rectangular mesh
- Fig.3 Flow chart (a) and program structure (b) of the SELENE code.
- Fig.4 Convergence of the scheme with respect to number of finite elements.  
(a)  $NDIV=MDIV=10$   
(b)  $NDIV=MDIV=20$   
(c)  $NDIV=MDIV=30$
- Fig.5 Convergence of eigenvalue  $\lambda$  and the safety factor at the magnetic axis ( $q_0$ ).
- Fig.6 Magnetic shears of large aspect ratio plasmas (numerical) and a cylindrical plasma (analytic).
- Fig.7 Examples of results for different values of  $\beta_J$ .  
(a)  $\beta_J=1$   
(b)  $\beta_J=2$   
(c)  $\beta_J=3$
- Fig.8 Examples of results for different values of scaling factor  $\sigma$ .  
(a)  $\sigma=0.028$   
(b)  $\sigma=0.030$   
(c)  $\sigma=0.032$   
(d)  $\sigma=0.034$   
(e)  $\sigma=0.036$

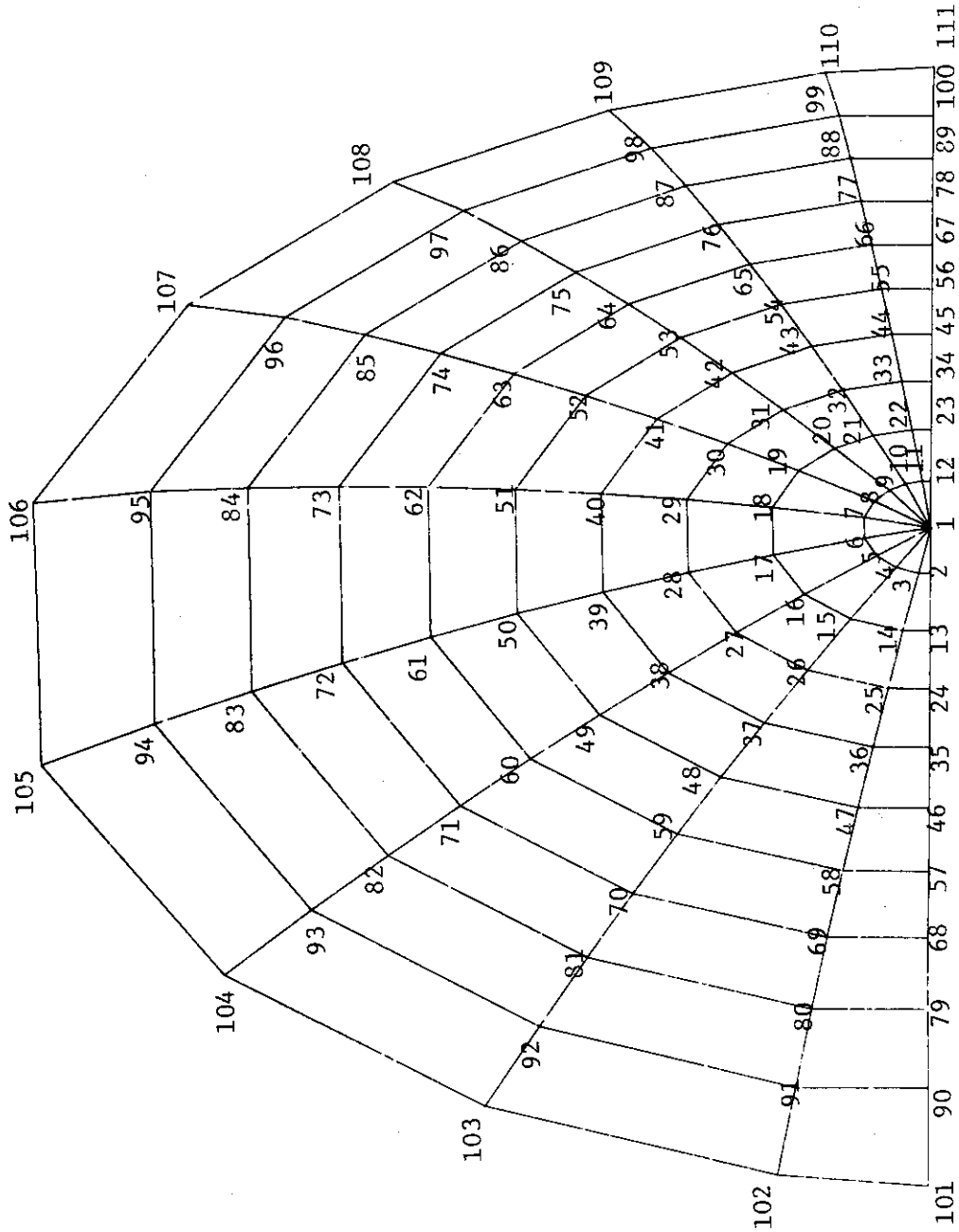
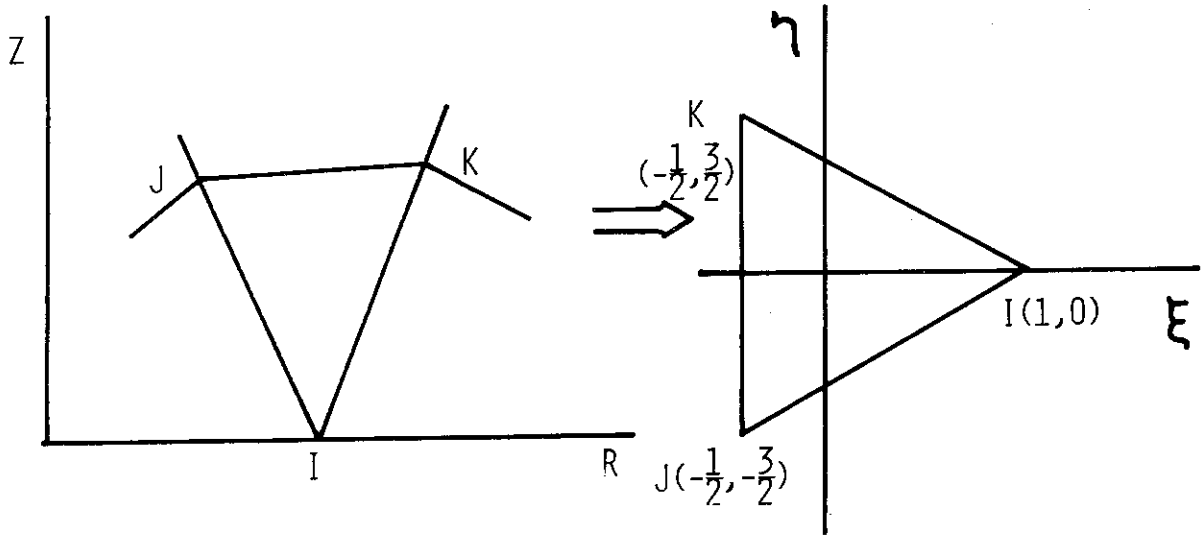
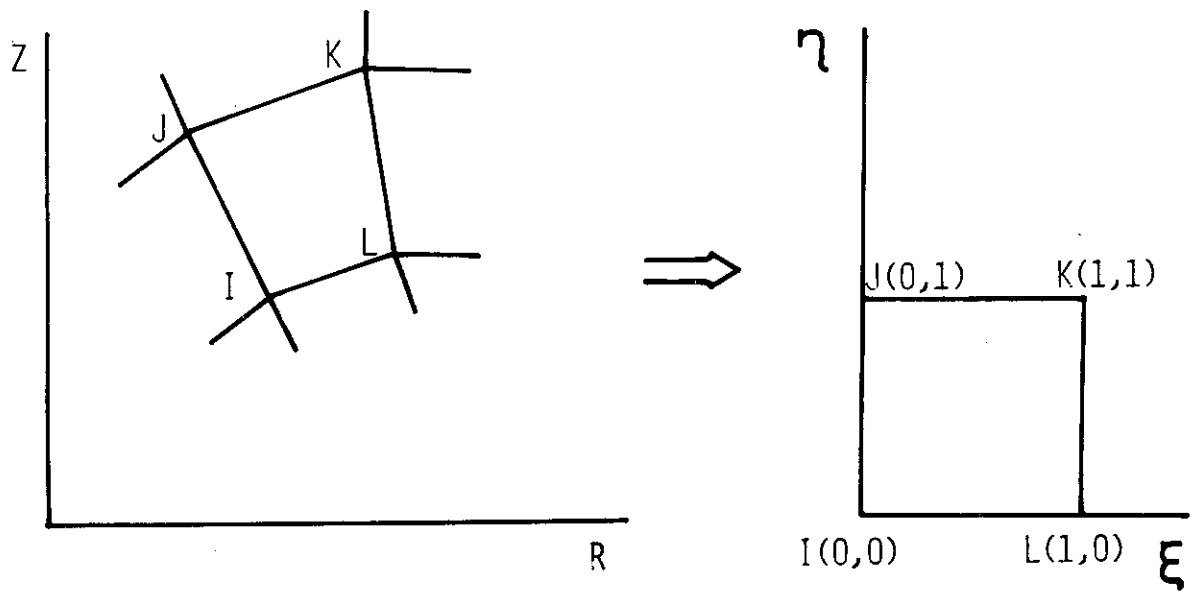


Fig.1 An example of mesh structure for equilibrium calculation.





(a)



(b)

Fig.2 Isoparametric transformation.

(a) A triangular mesh

(b) A rectangular mesh

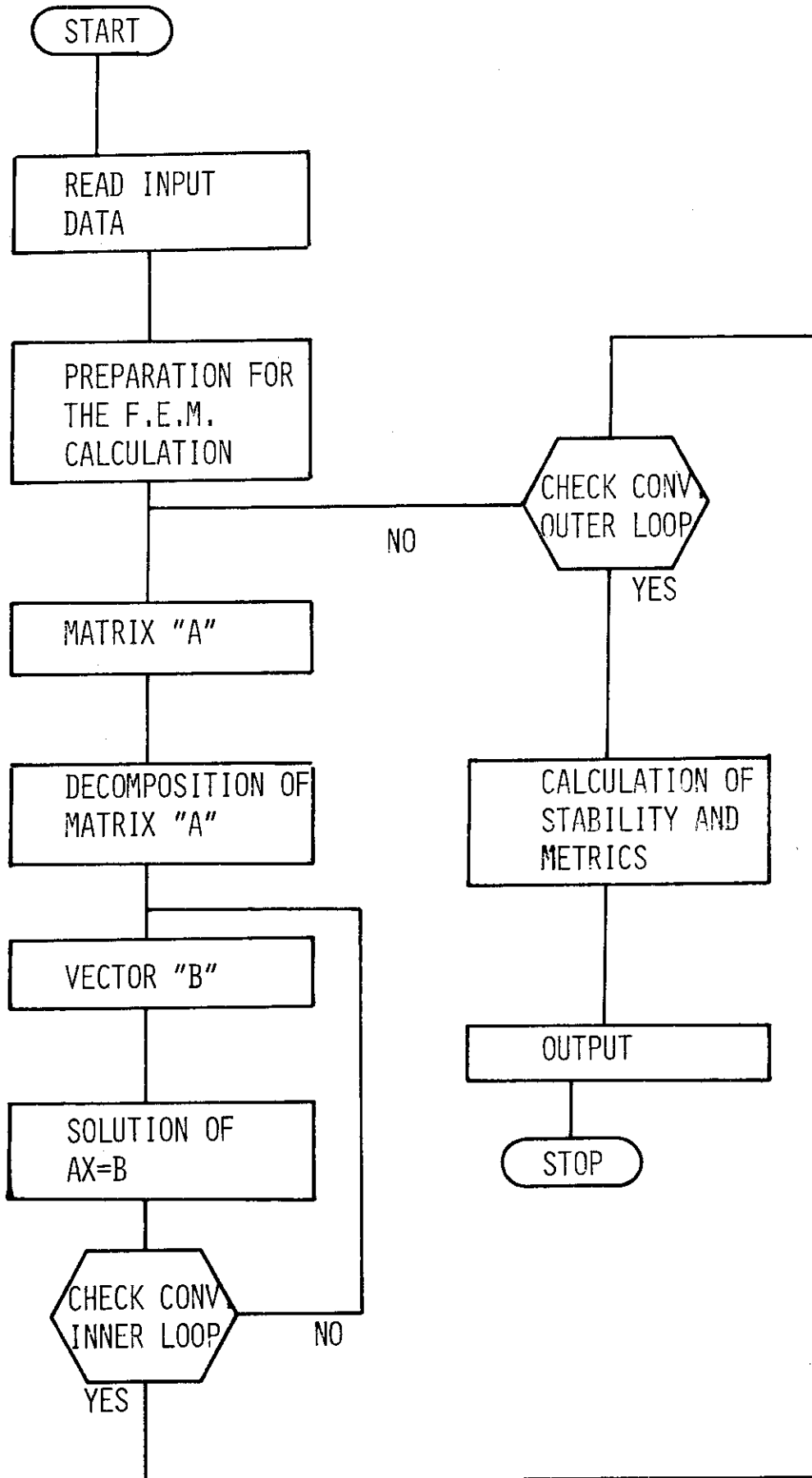


Fig.3 Flow chart (a) and program structure

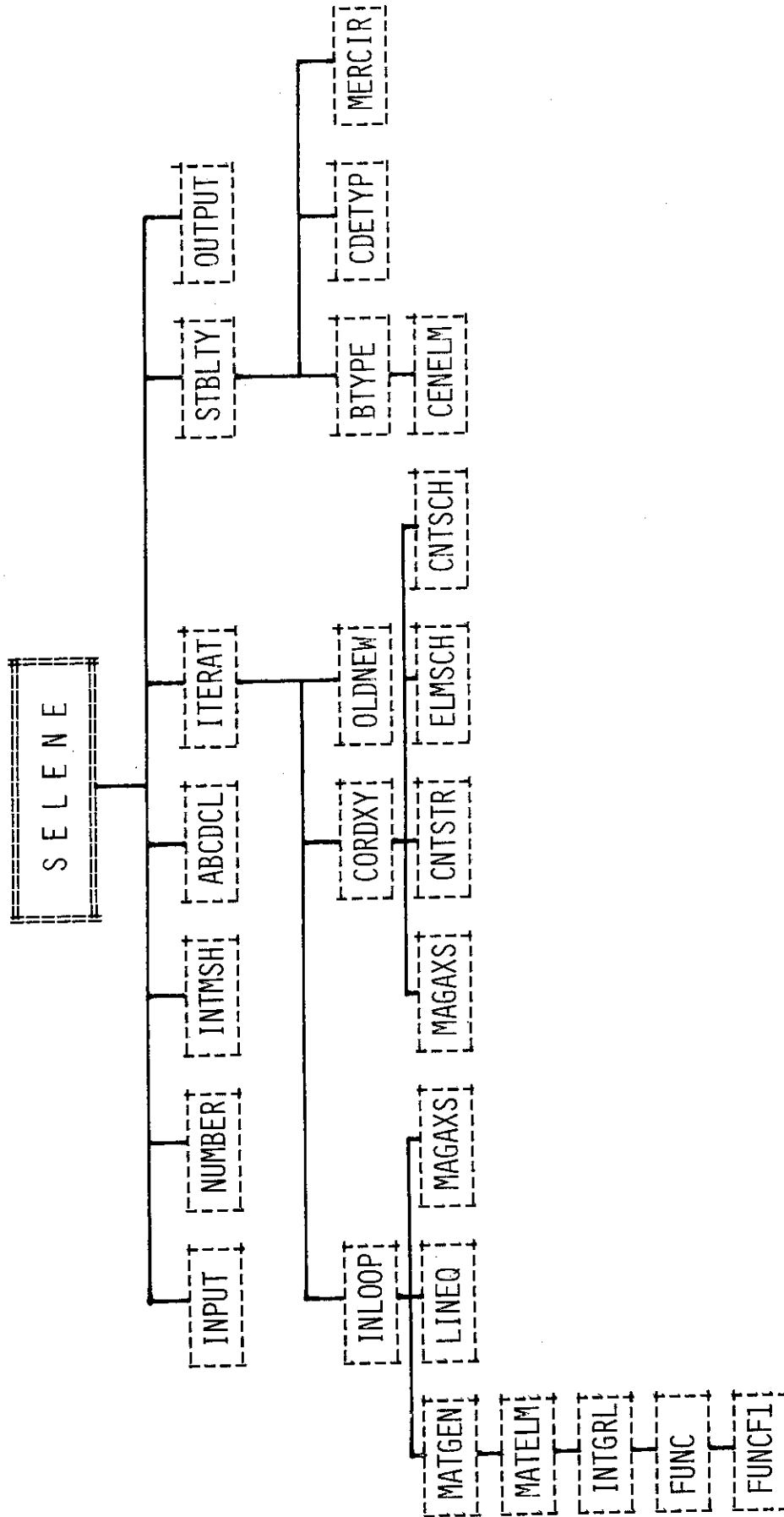


Fig. 3 Flow chart (b) of the SELENE code.

ITE=	5
NDIV=	10
MDIV=	10
RC=	1.0
A=	3.30
E=	1.70
D=	0.00
ALPHA=	0.70
BETAJ=	1.50
L=	4
LAMDA=	61.40
DAXIS=	1.020

DATE= 78-09-27  
TIME= 15-43-0

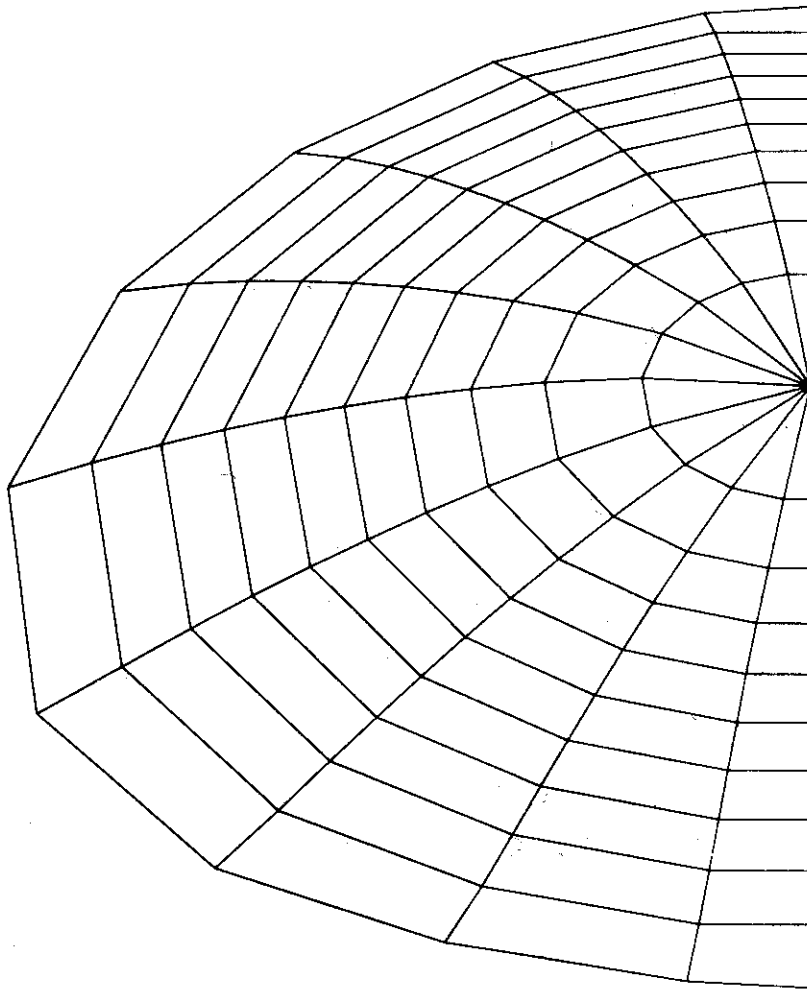


Fig.4 Convergence of the scheme with respect to number of finite elements. (a) NDIV=MDIV=10



ITE=	5
NDIV=	20
MDIV=	20
RC=	1.0
A=	3.30
E <sub>0</sub> =	1.70
D=	0.00
ALPHA=	0.70
BETAJ=	1.50
L=	4
LAMDA=	59.56
DAXIS=	1.022

DATE= 78-09-27  
TIME= 14-55-4

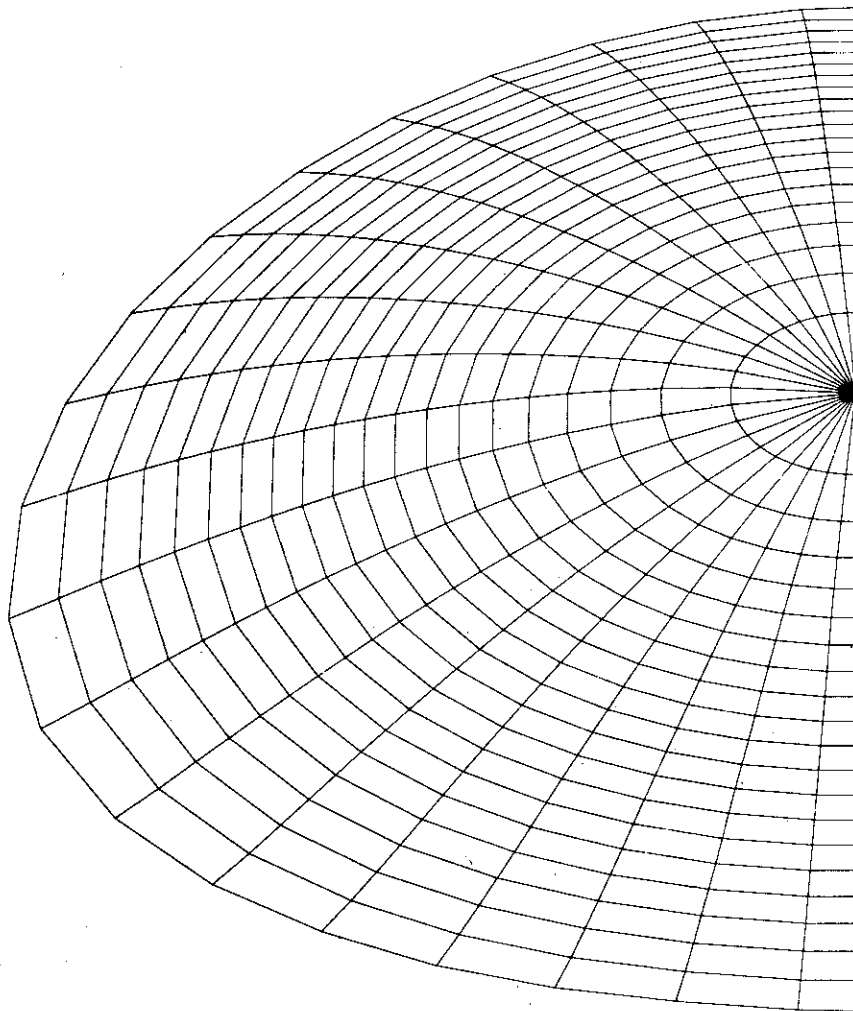


Fig.4 Convergence of the scheme with respect to number of finite elements. (b) NDIV=MDIV=20



ITE=	5
NDIV=	30
MDIV=	30
RC=	1.0
A=	3.30
E=	1.70
D=	0.00
ALPHA=	0.70
BETAJ=	1.50
L=	4
LAMDA=	59.23
DAXIS=	1.022

DATE= 78-09-29  
TIME= 9-34-48

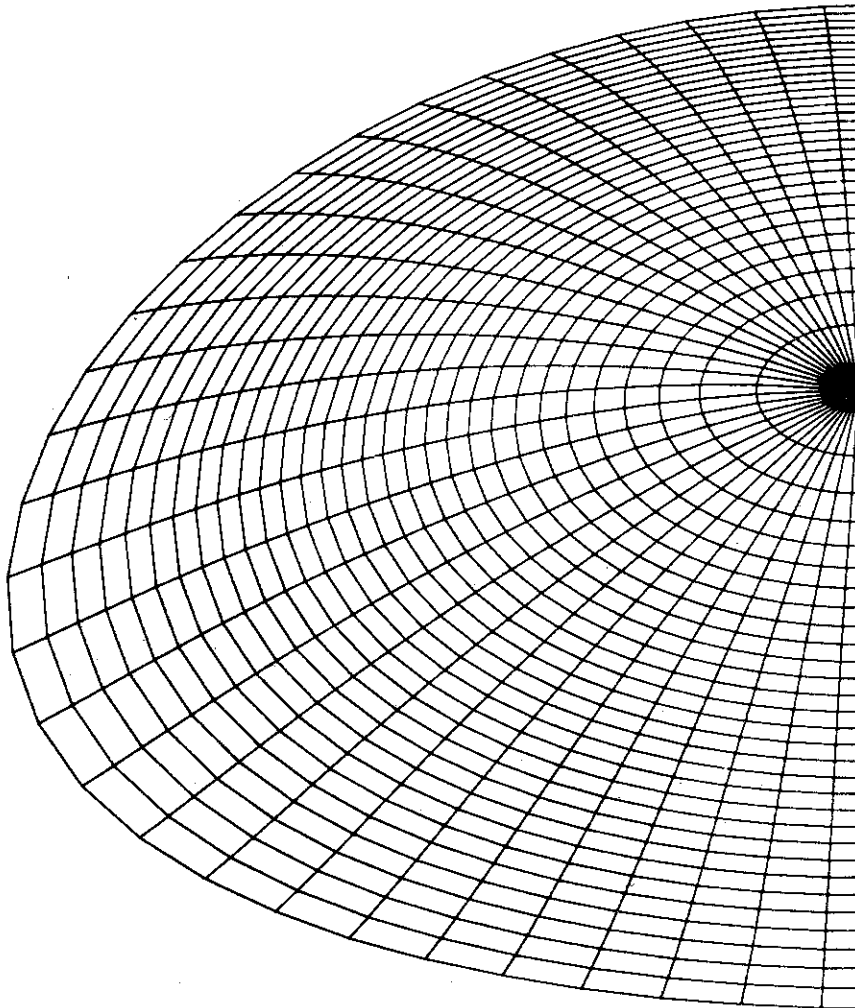


Fig.4 Convergence of the scheme with respect to number of finite elements. (c) NDIV=MDIV=30

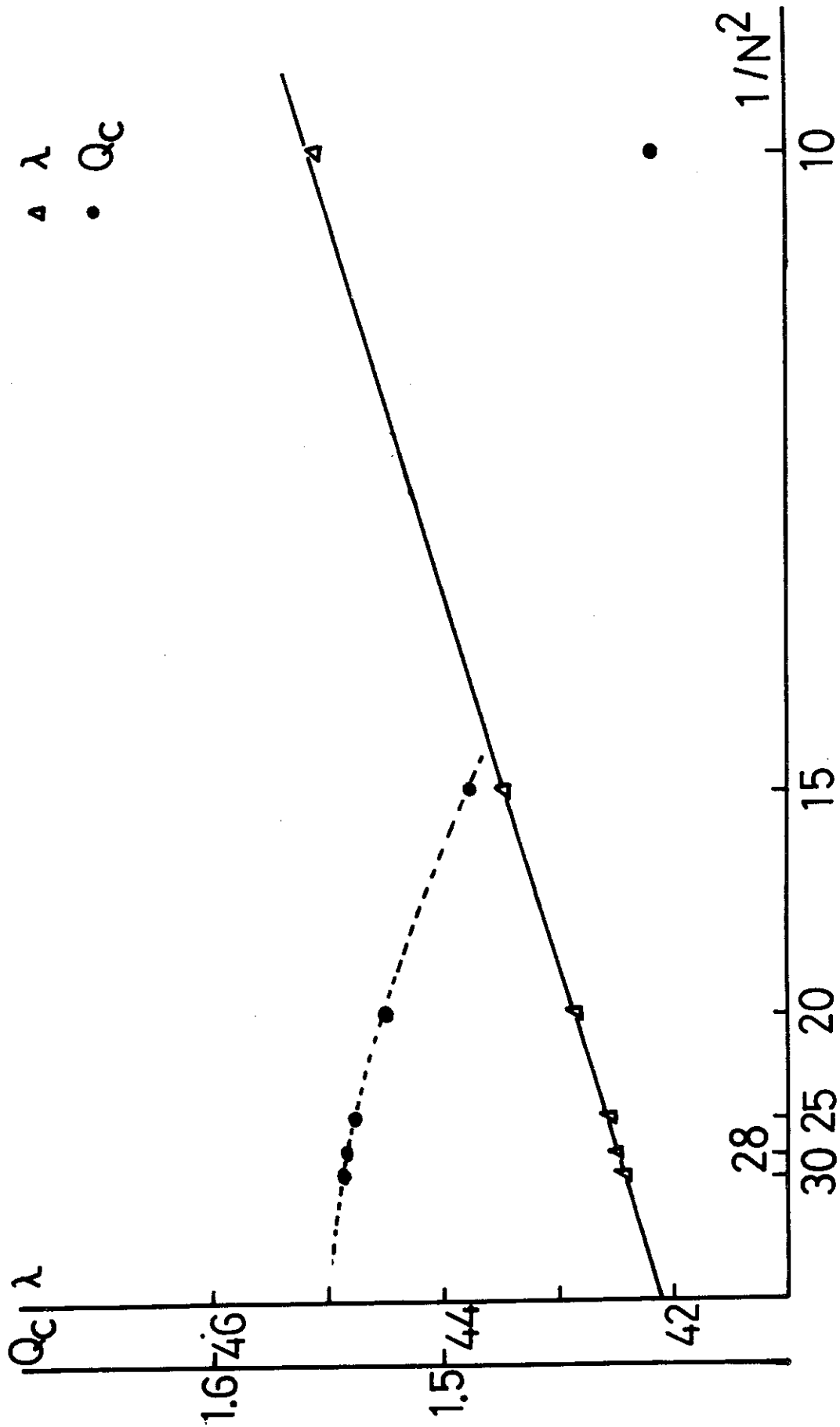


Fig.5 Convergence of eigenvalue  $\lambda$  and the safety factor at the magnetic axis ( $q_0$ ).

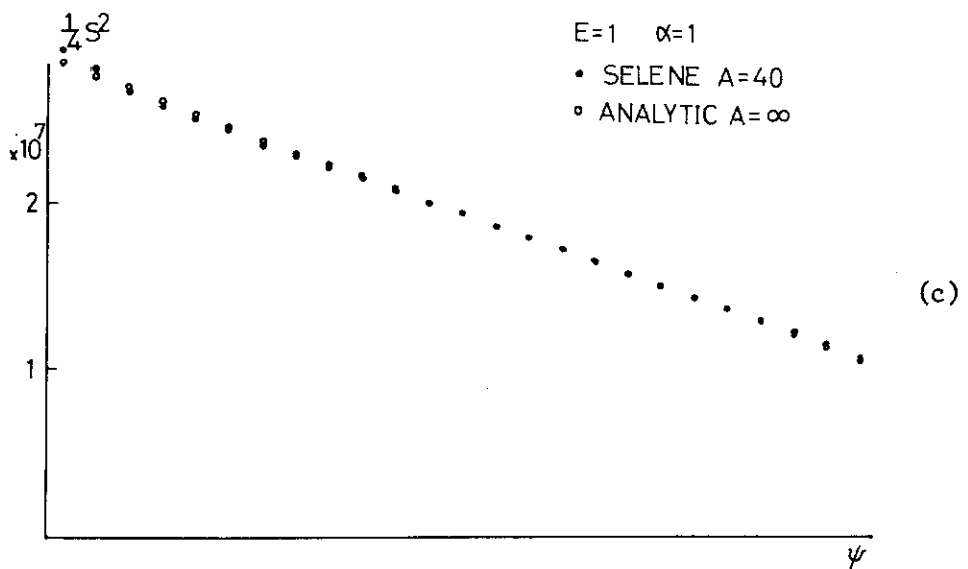
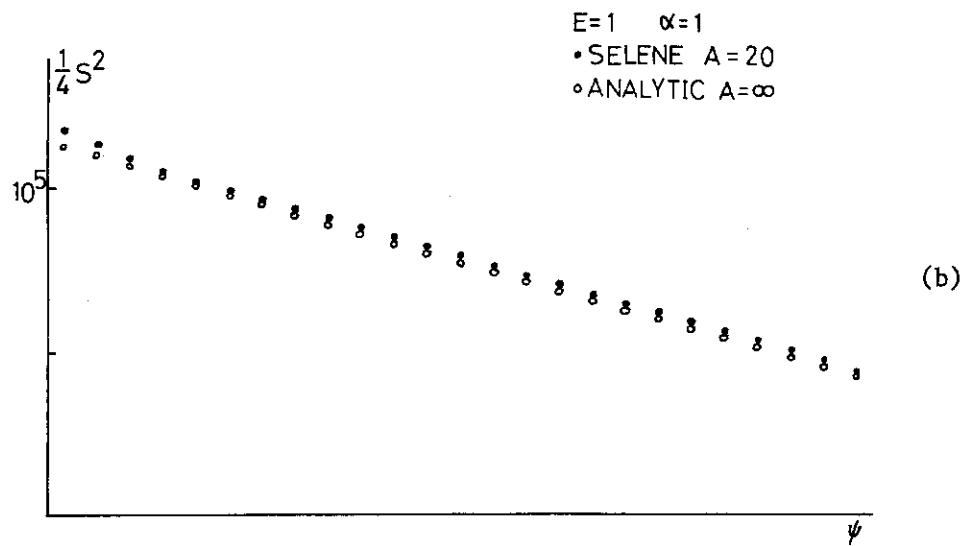
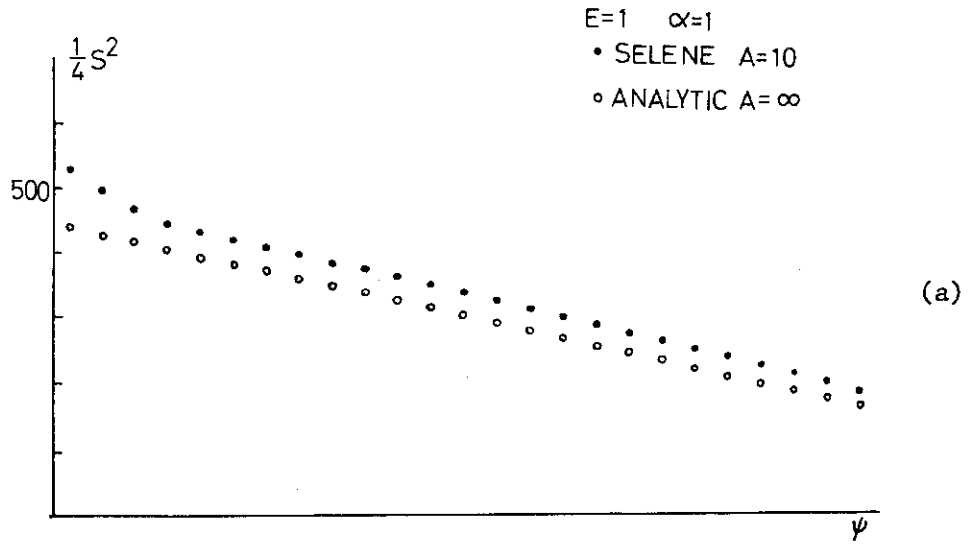


Fig.6 Magnetic shears of large aspect ratio plasmas(numerical) and a cylindrical plasma(analytic).



ITE=	7
NDIV=	25
MDIV=	25
RC=	1.0
R=	3.30
E=	1.70
D=	0.00
ALPHA=	1.03
BETAJ=	1.00
L=	4
LAMDAR=	42.57
DAXIS=	1.051

DATE= 78-09-27  
 TIME= 10-25-49

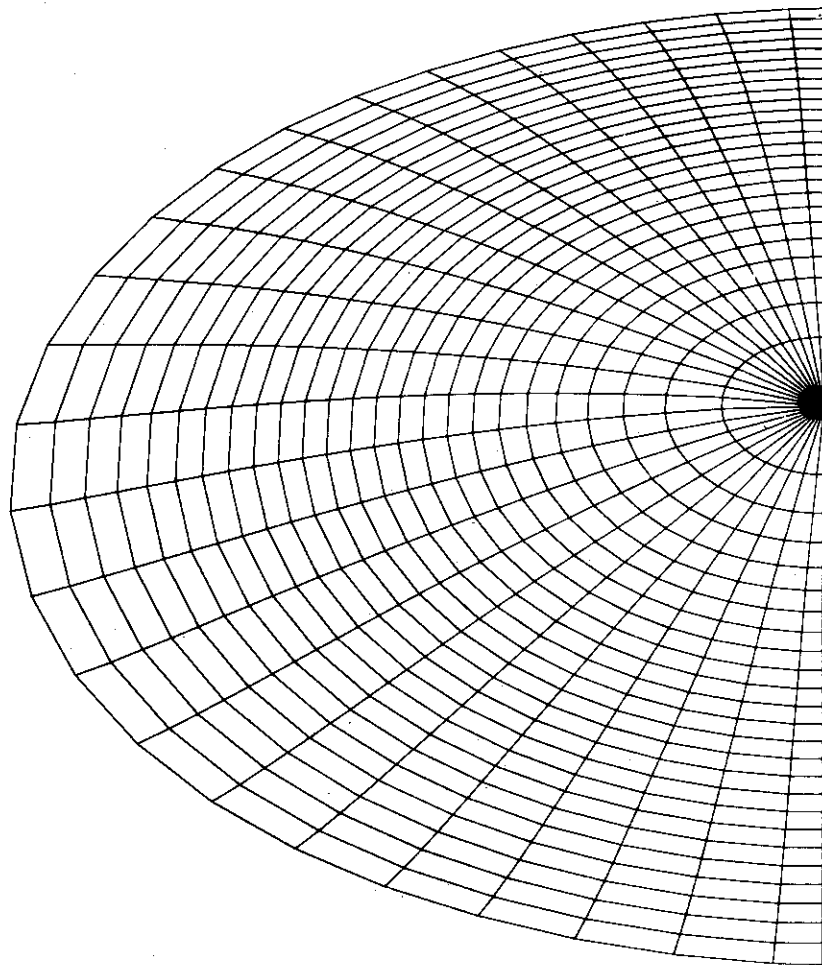


Fig.7 Examples of results for different values of  $\beta_J$ . (a)  $\beta_J=1$

# PARAMETERS

ISIGMA= 5  
ISTOT= 0  
QC= 1.55  
SIGMA= 0.0280  
BETA= 0.0071  
BETAP= 0.895  
BETAST= 0.0108

Q-PROFILE  
MAX= 5.83 E0  
MIN= 1.55 E0  
SECT= 1.E 0

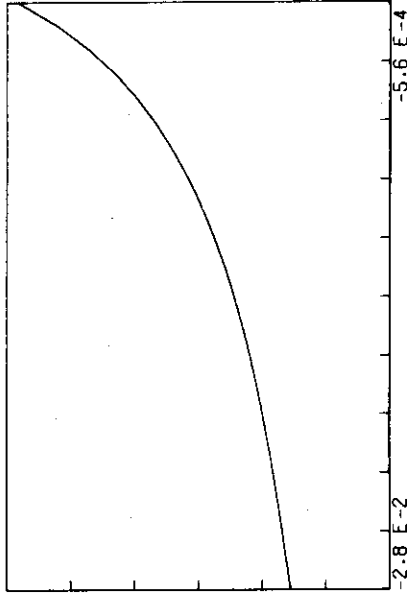


Fig. 7 (a-2)

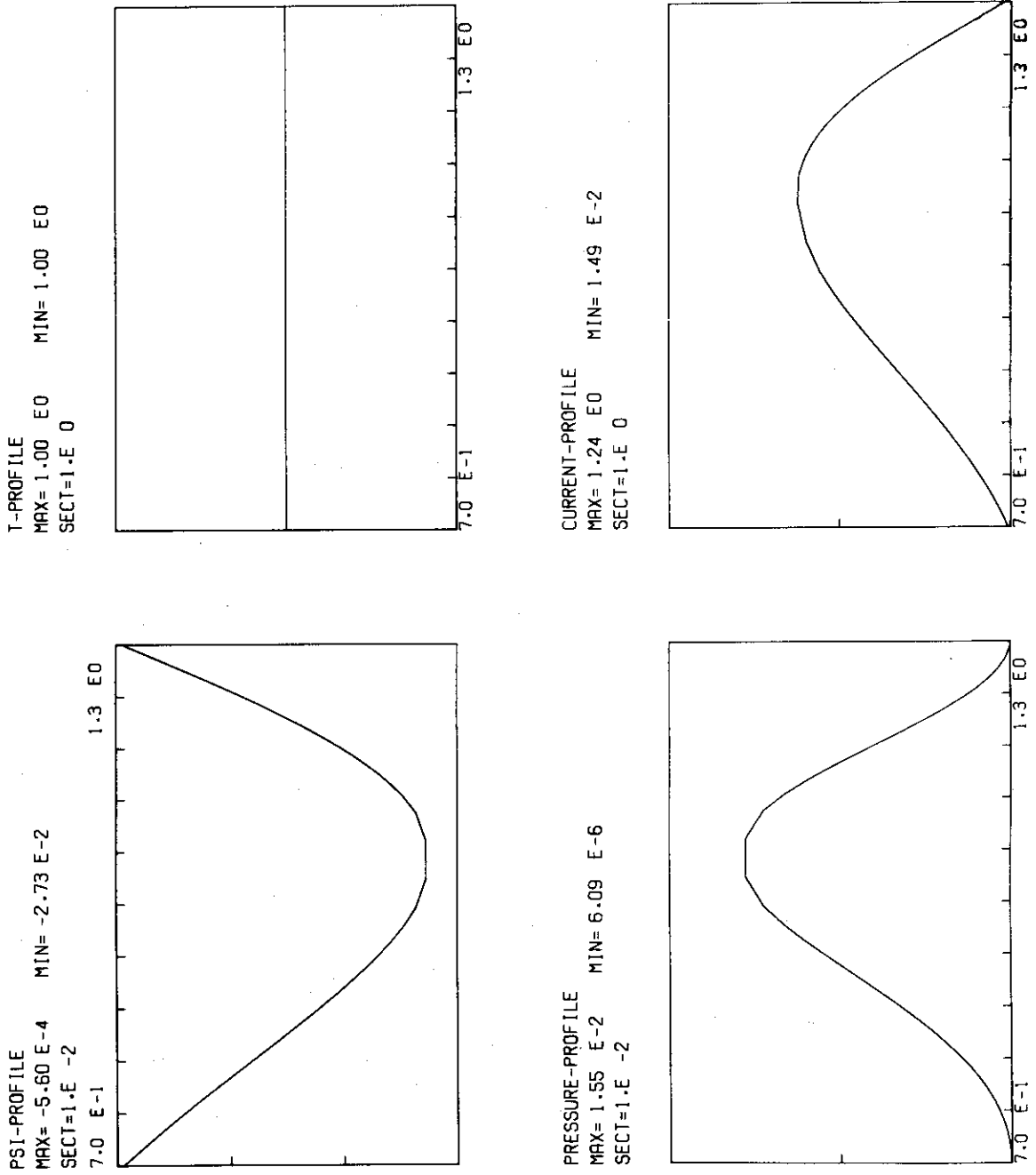


Fig. 7 (a-3)

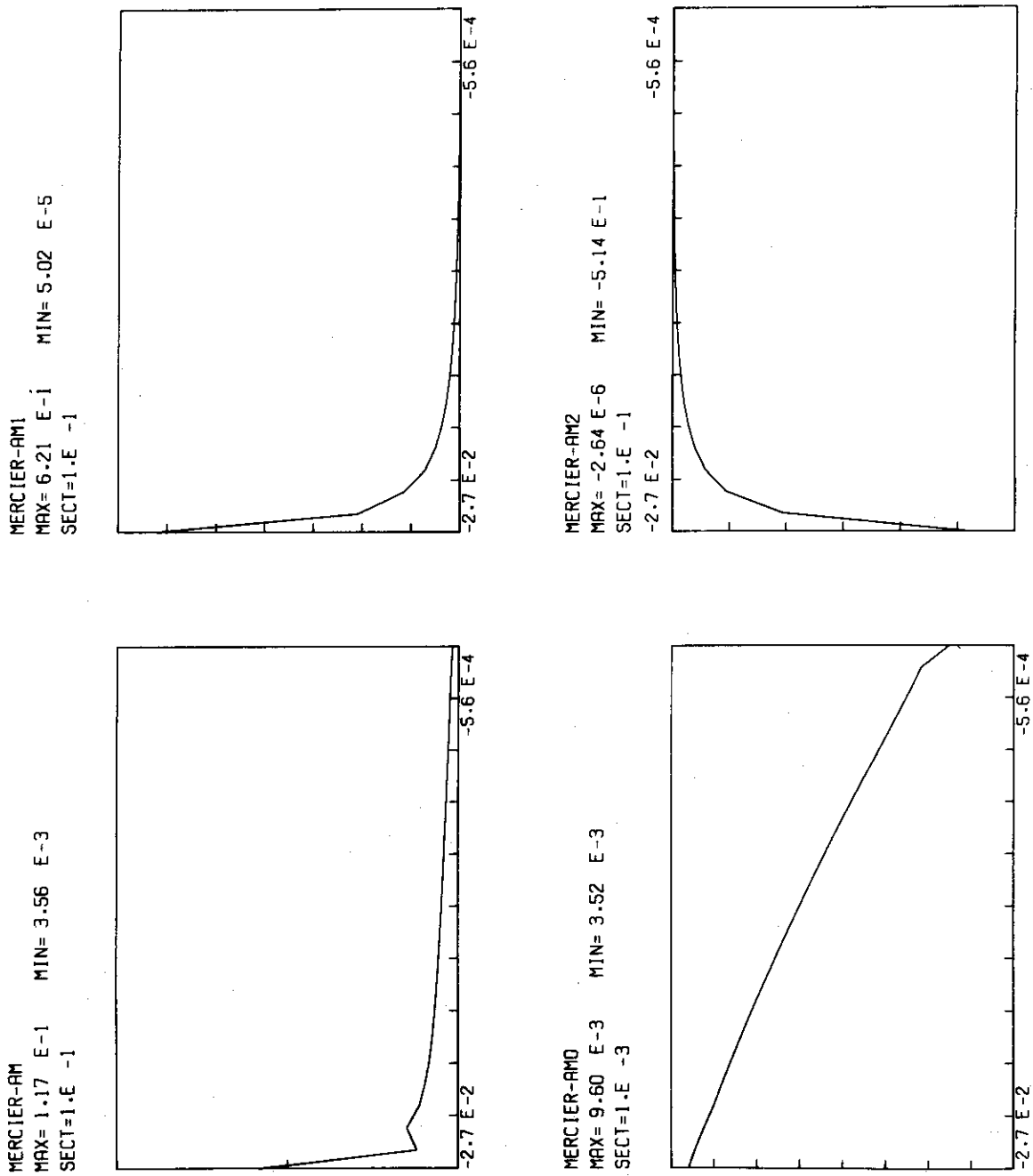
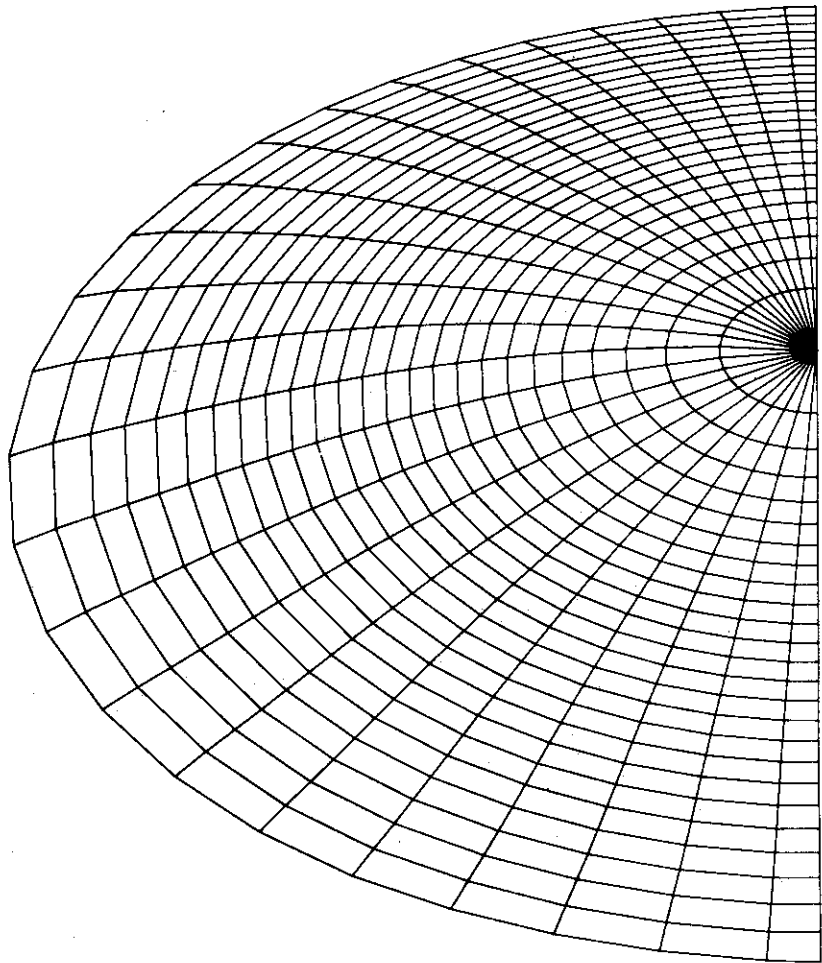


Fig. 7 (a-4)

ITE=	7
NDIV=	25
MDIV=	25
RC=	1.0
A=	3.30
E=	1.70
D=	0.00
ALPHA=	1.03
BETAJ=	2.00
L=	4
LAMDA=	94.25
DAXIS=	1.085

DATE= 78-09-27  
TIME= 11-40-23



(b)  $\beta_J=2$

Fig.7 Examples of results for different values of  $\beta_J$ .

# PARAMETERS

ISIGMA= 5  
ISTOT= 0  
QC= 1.29  
SIGMA= 0.0280  
BETA= 0.0140  
BETAP= 2.063  
BETAST= 0.0219

Q-PROFILE  
MAX= 7.00 E0    MIN= 1.29 E0  
SECT= 1.E 0

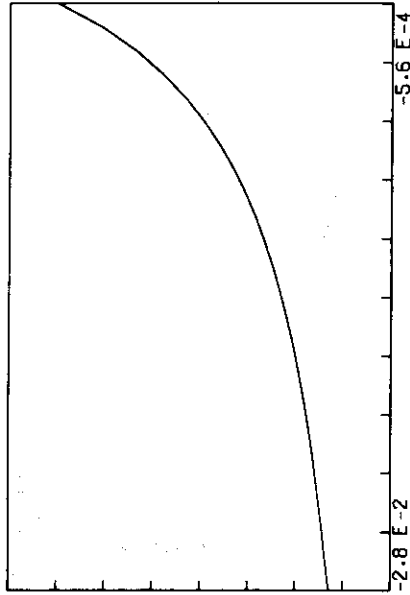
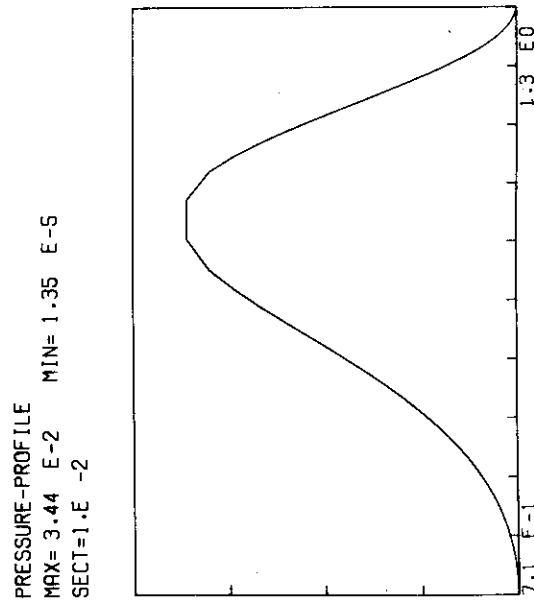
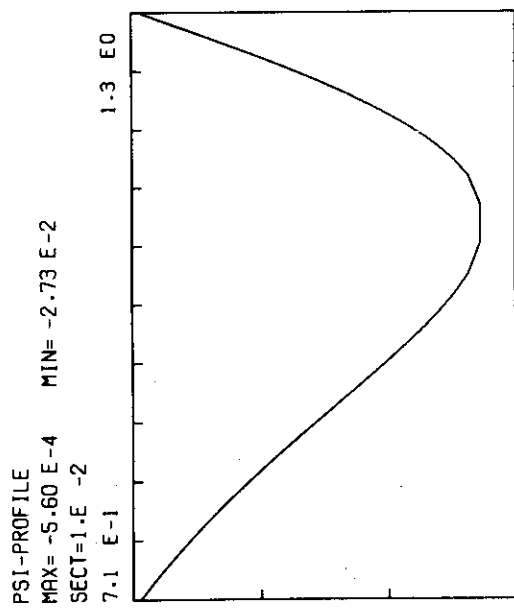
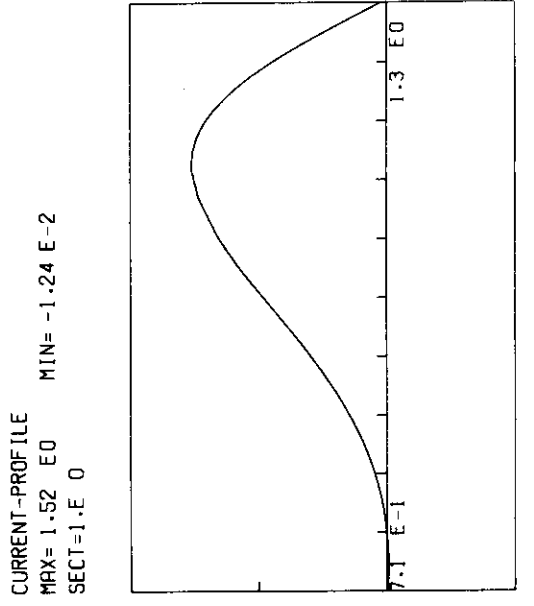
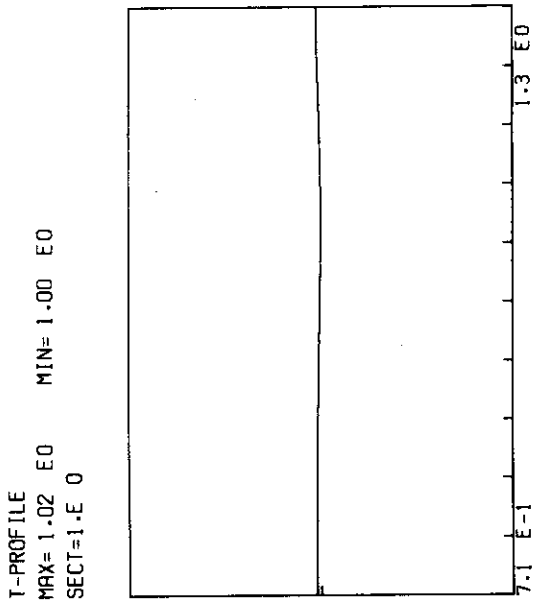


Fig. 7 (b-2)



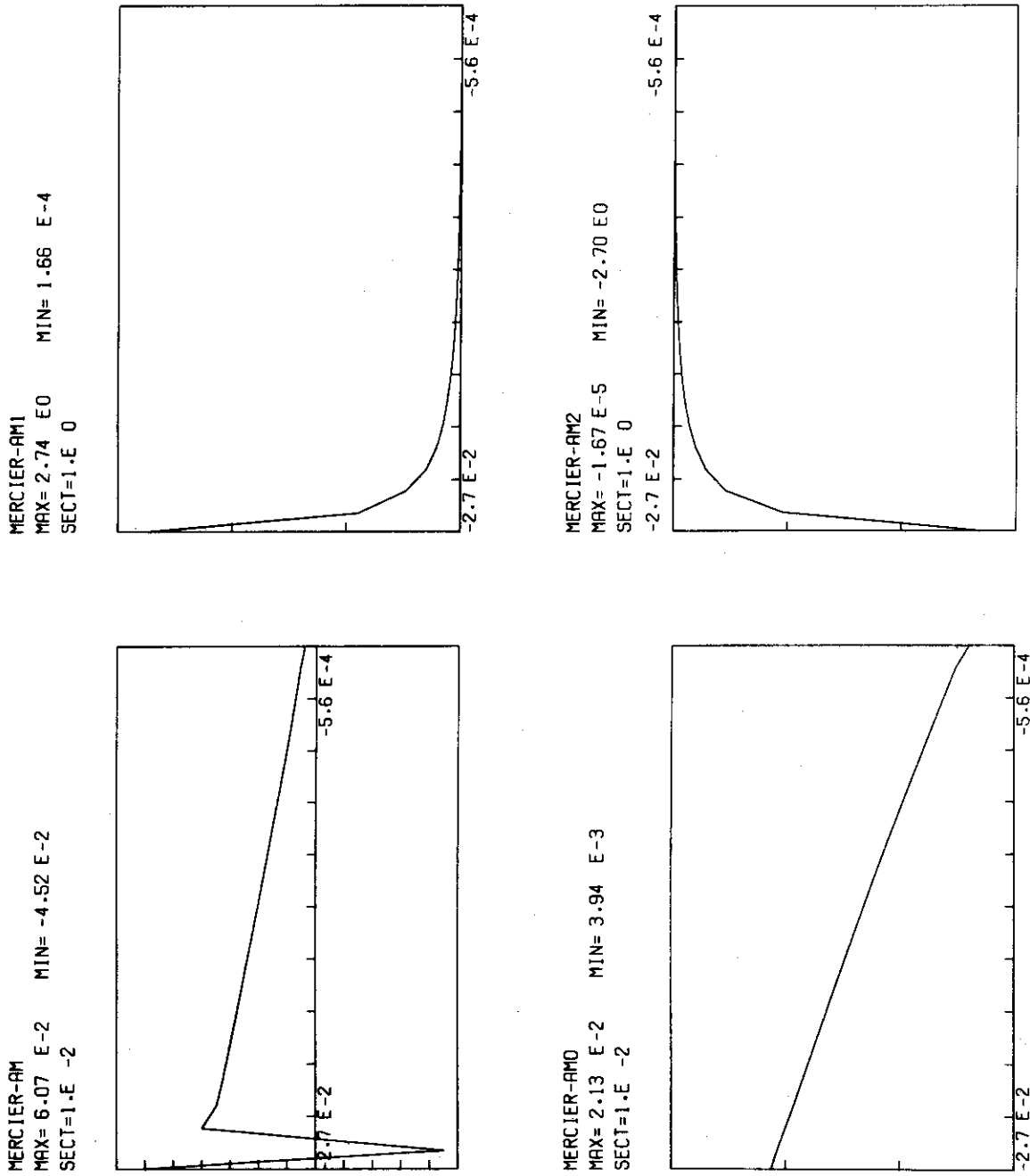


Fig. 7 (b-4)



ITE=	7
NOIV=	25
MOIV=	25
RC=	1.0
A=	3.30
E=	1.70
D=	0.00
ALPHA=	1.03
BETAJ=	3.00
L=	4
LAMDA=	173.28
OAXIS=	1.119

DATE= 78-09-27  
TIME= 11 - 4 - 45

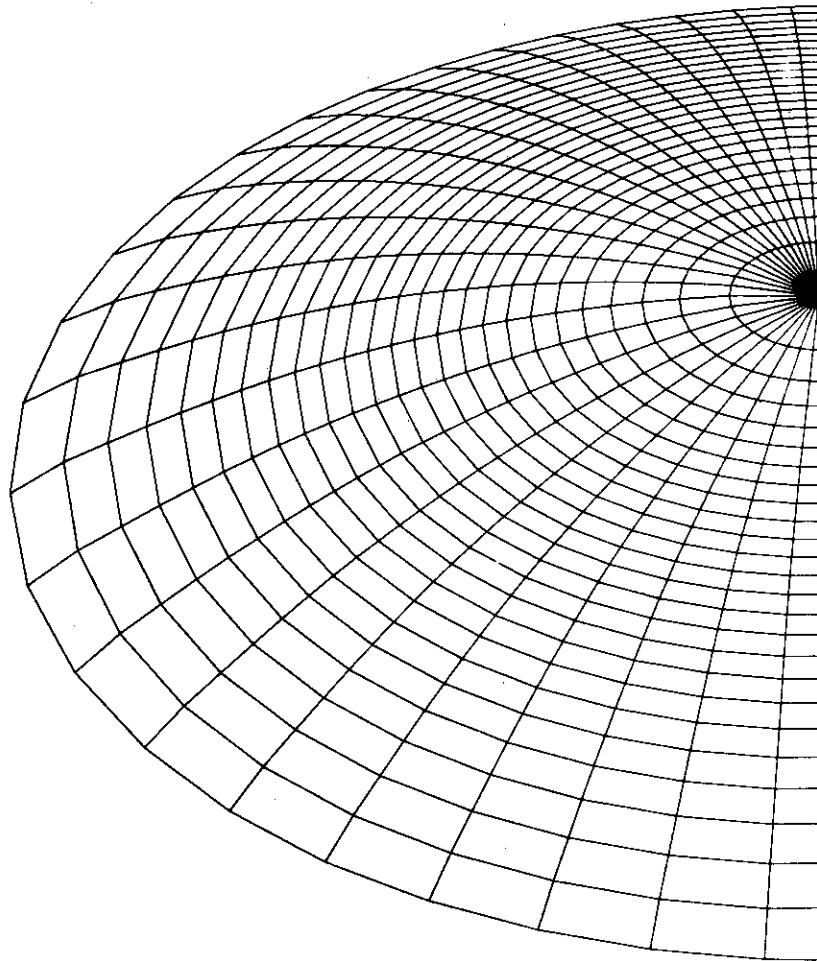


Fig.7 Examples of results for different values of  $\beta_J$ . (c)  $\beta_J=3$

# PARAMETERS

ISIGMA= 5  
ISTOT= 0  
QC= 0.99  
SIGMA= 0.0280  
BETA= 0.0204  
BETAP= 3.881  
BETAST= 0.0343

Q-PROFILE  
MAX= 1.01 E1  
MIN= 9.86 E-1  
SECT= 1. E 1

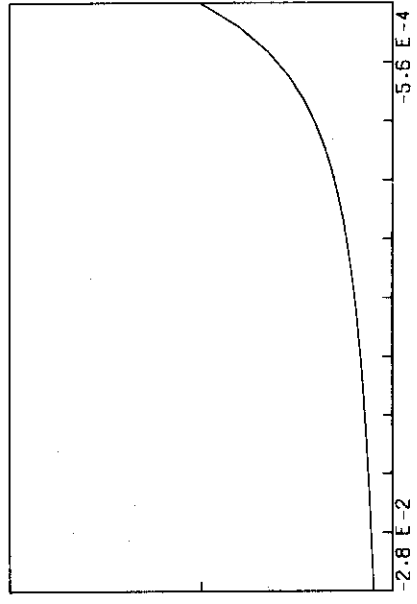
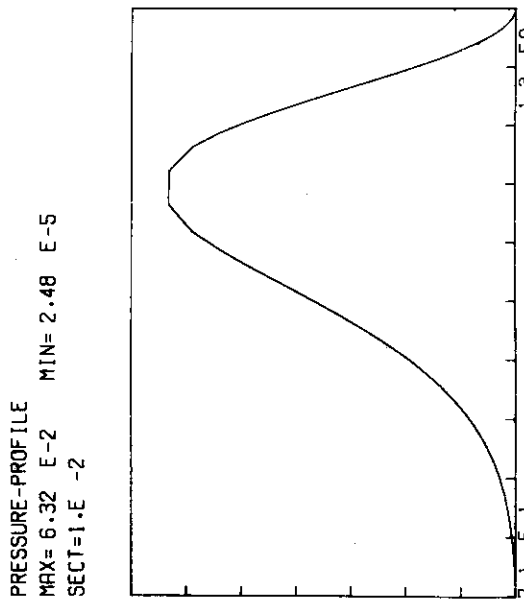
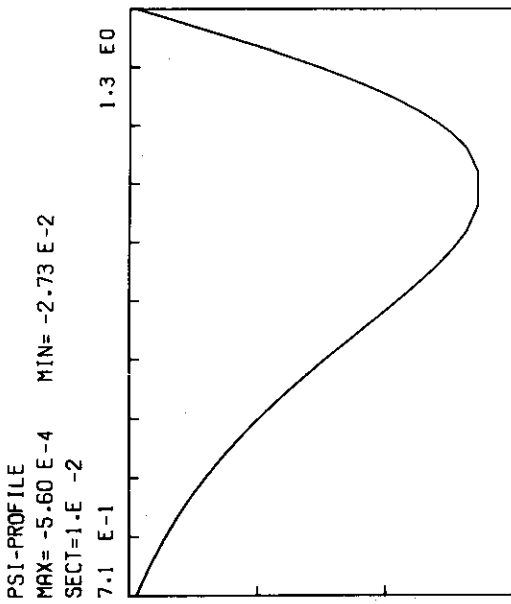
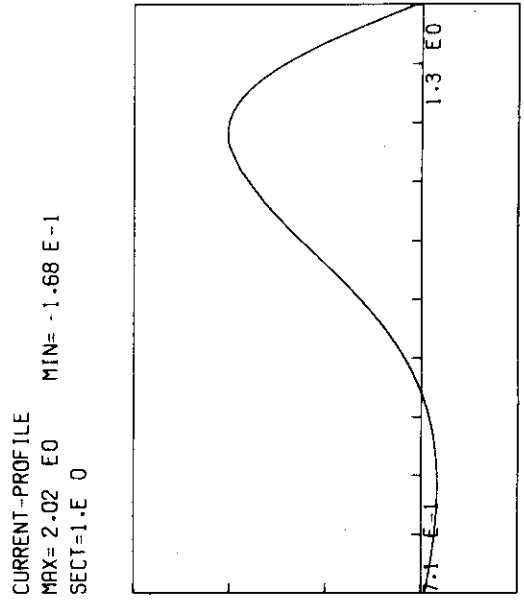
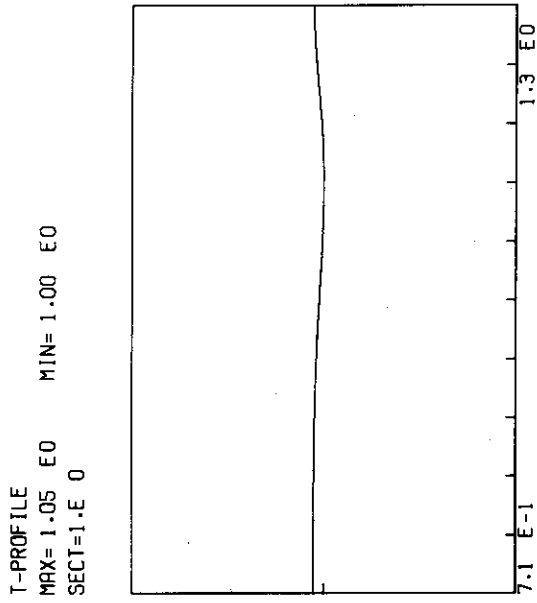


Fig. 7 (c-2)



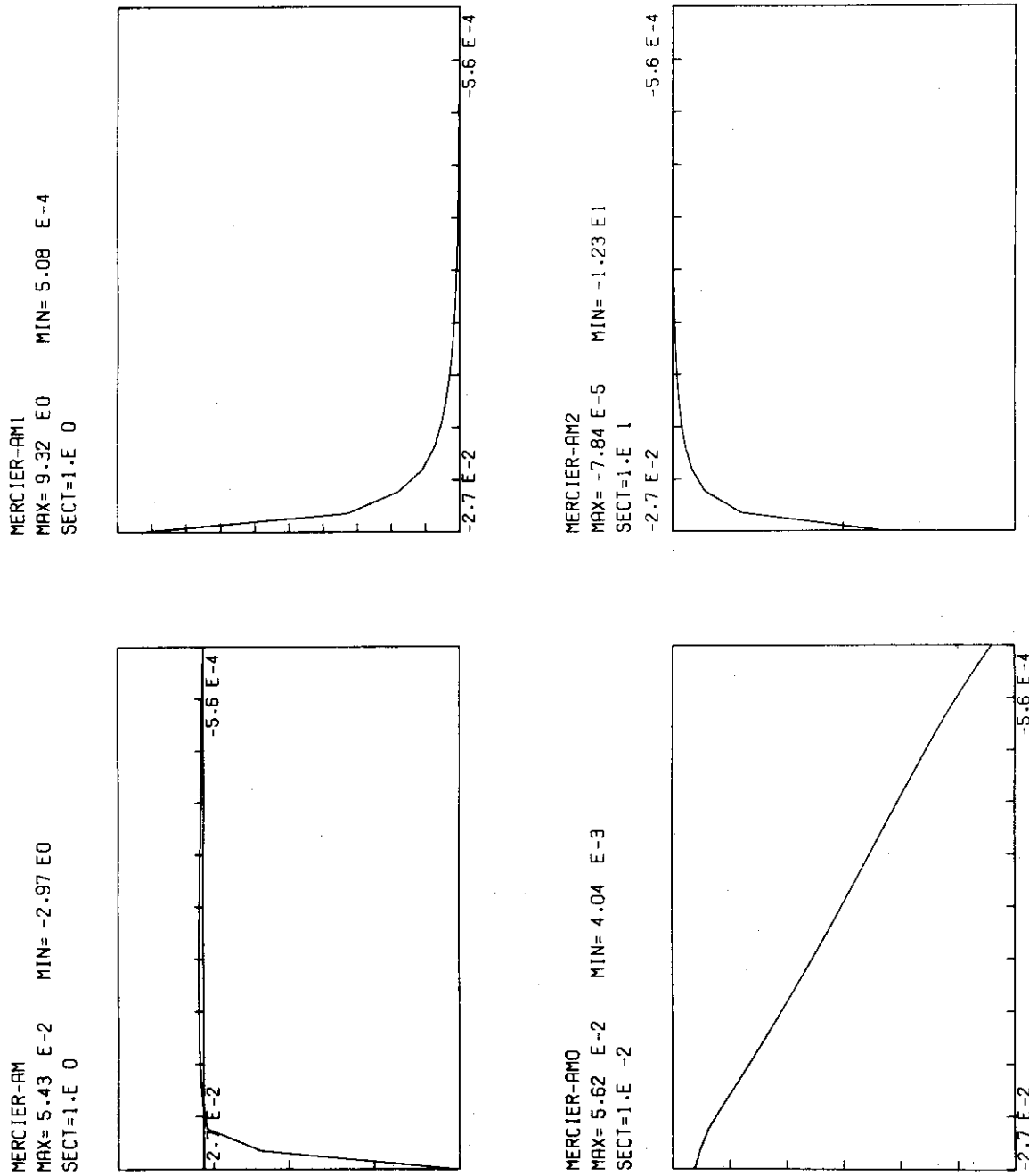


Fig. 7 (c-4)

ITE=	7
NOIV=	25
MOIV=	25
RC=	1.0
A=	3.30
E=	1.70
D=	0.00
ALPHA=	1.03
BETAJ=	1.00
L=	4
LAMDA=	42.57
OAXIS=	1.051

DATE= 78-09-28  
TIME= 22 - 3 - 57

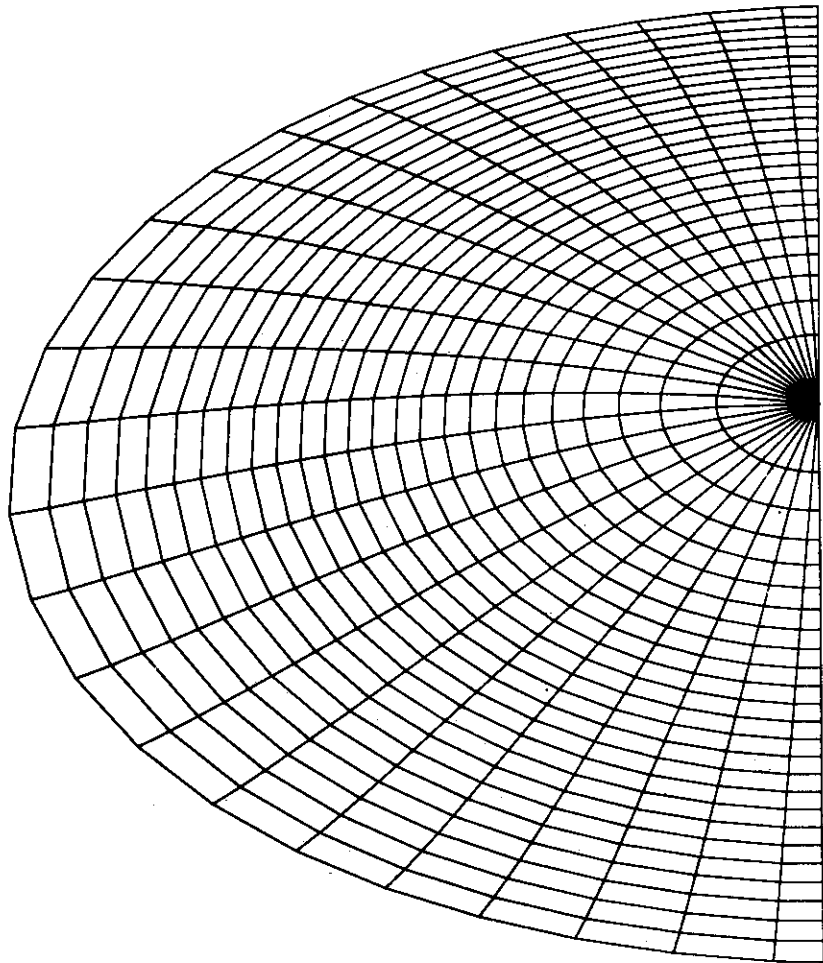


Fig.8 Examples of results for different values of scaling factor  $\sigma$ .

# PARAMETERS

ISIGMA= 5  
 ISTOT= 0  
 QC= 1.55  
 SIGMA= 0.0280  
 BETA= 0.0071  
 BETAP= 0.895  
 BETAST= 0.0108

Q-PROFILE  
 MAX= 5.83 E0  
 MIN= 1.55 E0  
 SECT= 1.E 0

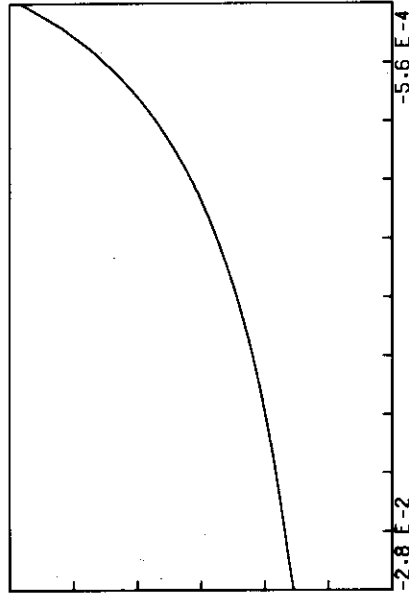


Fig.8 Examples of results for different values of scaling factor  $\sigma$ .  
 (a)  $\sigma=0.028$

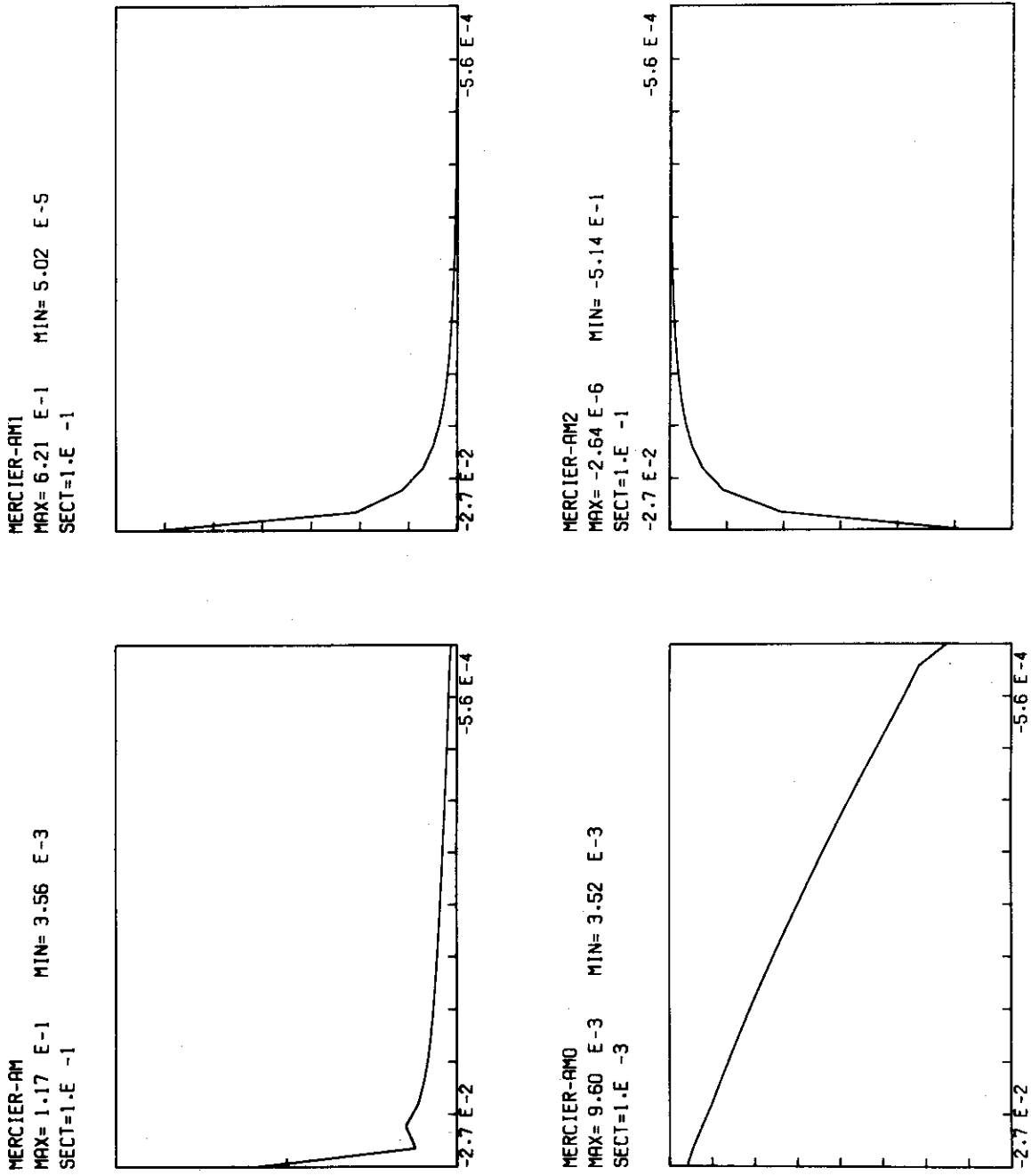


Fig. 8 (a-2)

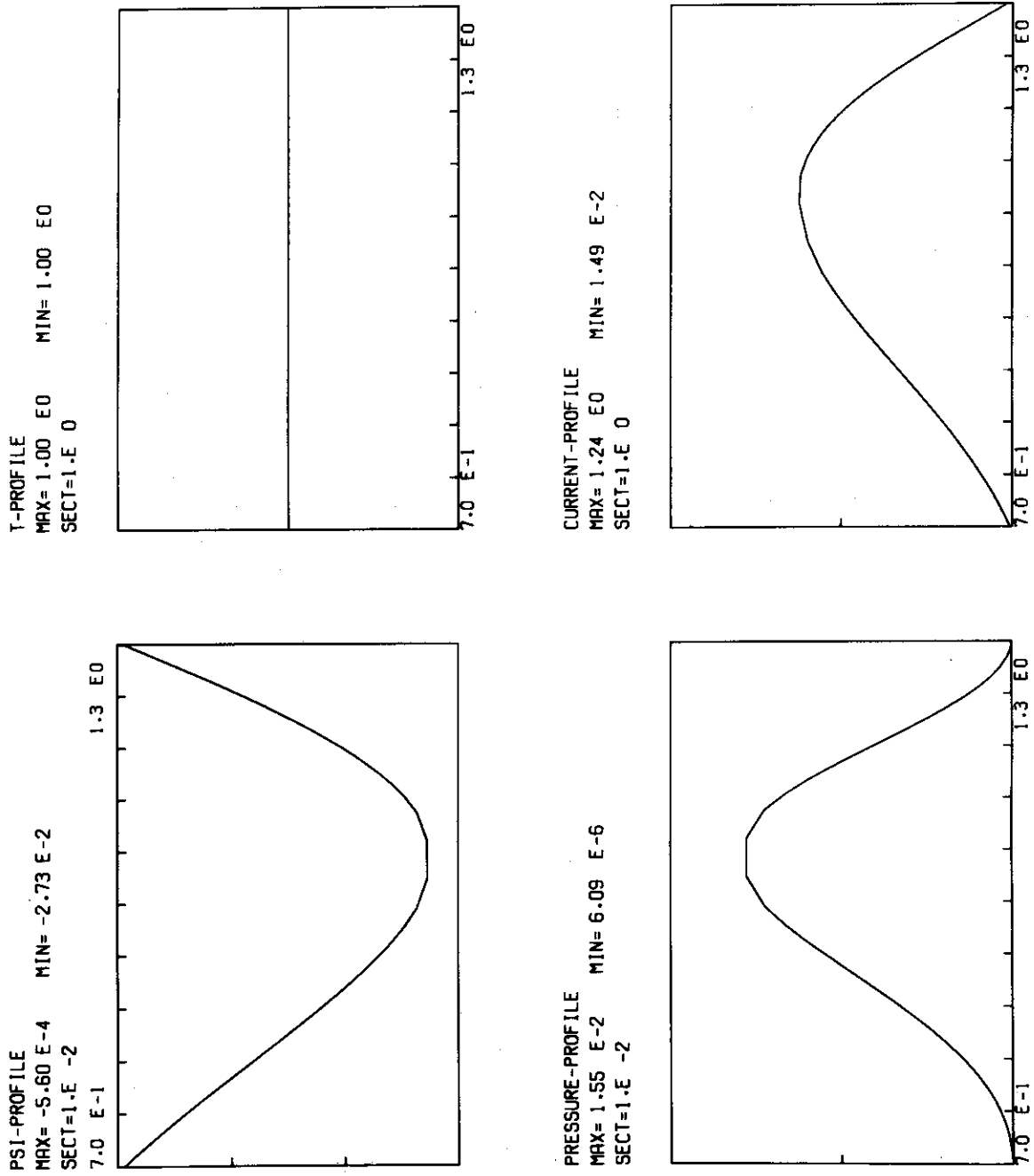


Fig. 8 (a-3)



# PARAMETERS

ISIGMA= 5  
 ISTOT= 1  
 QC= 1.45  
 SIGMA= 0.0300  
 BETA= 0.0082  
 BETAP= 0.895  
 BETAST= 0.0124

Q-PROFILE  
 MAX= 5.44 E0  
 MIN= 1.45 E0  
 SECT= 1.E 0

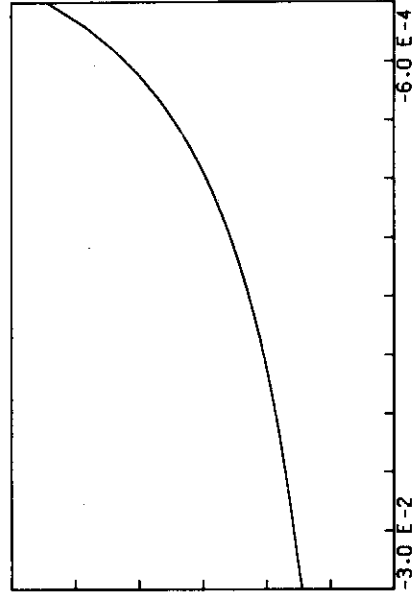


Fig.8 Examples of results for different values of scaling factor  $\sigma$ .

(b)  $\sigma=0.030$



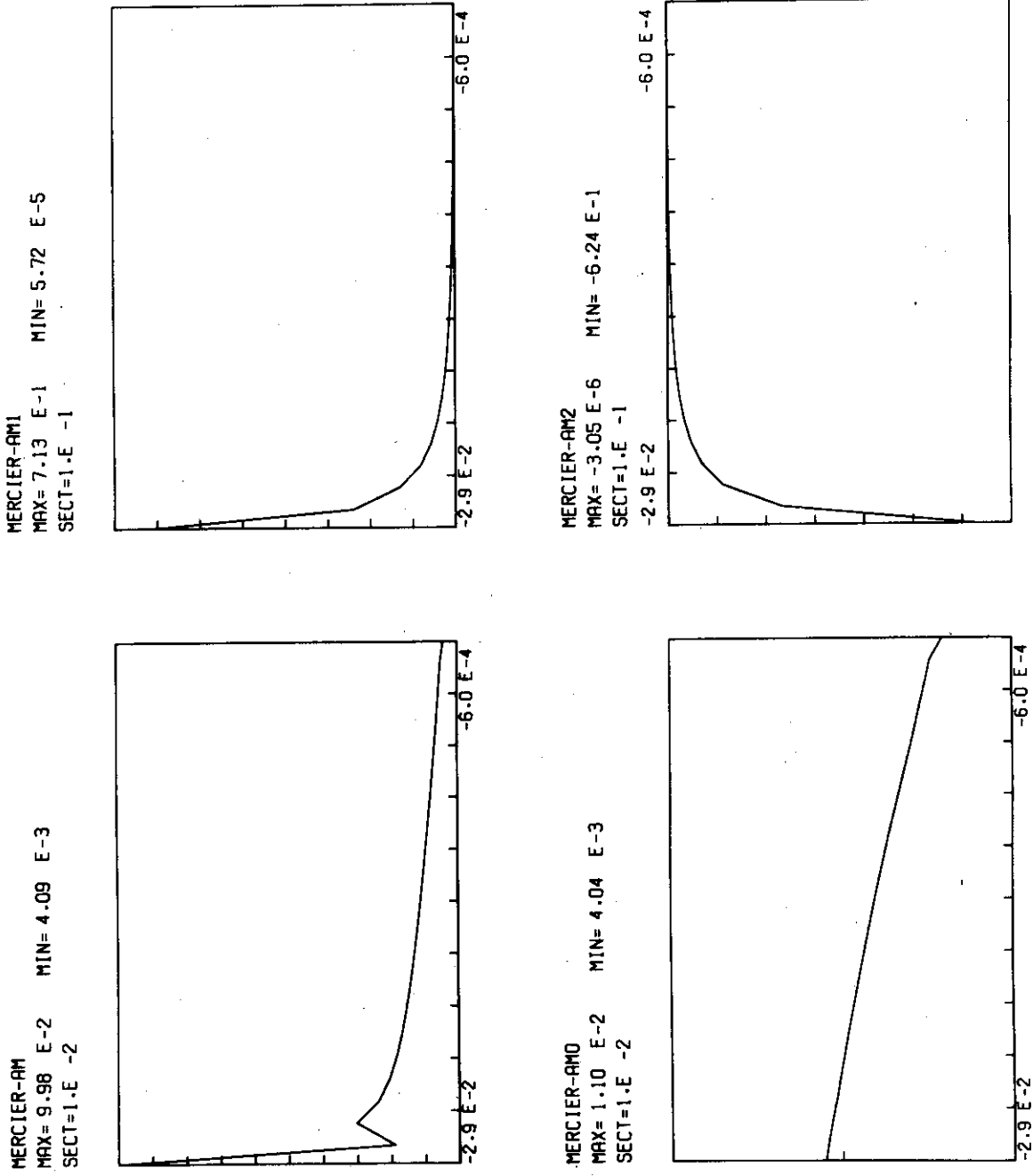


Fig. 8 (b-3)

# PARAMETERS

```

ISIGMA= 5
ISTOT= 2
QC= 1.36
SIGMA= 0.0320
BETA= 0.0093
BETAP= 0.895
BETAST= 0.0141
    
```

Q-PROFILE  
 MAX= 5.10 E0  
 MIN= 1.36 E0  
 SECT= 1.E 0

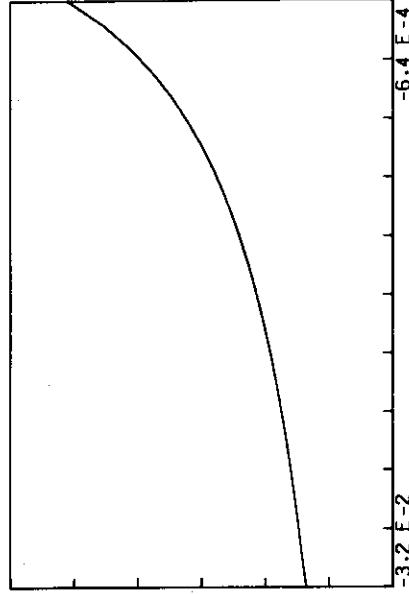


Fig.8 Examples of results for different values of scaling factor  $\sigma$ .  
 (c)  $\sigma=0.032$

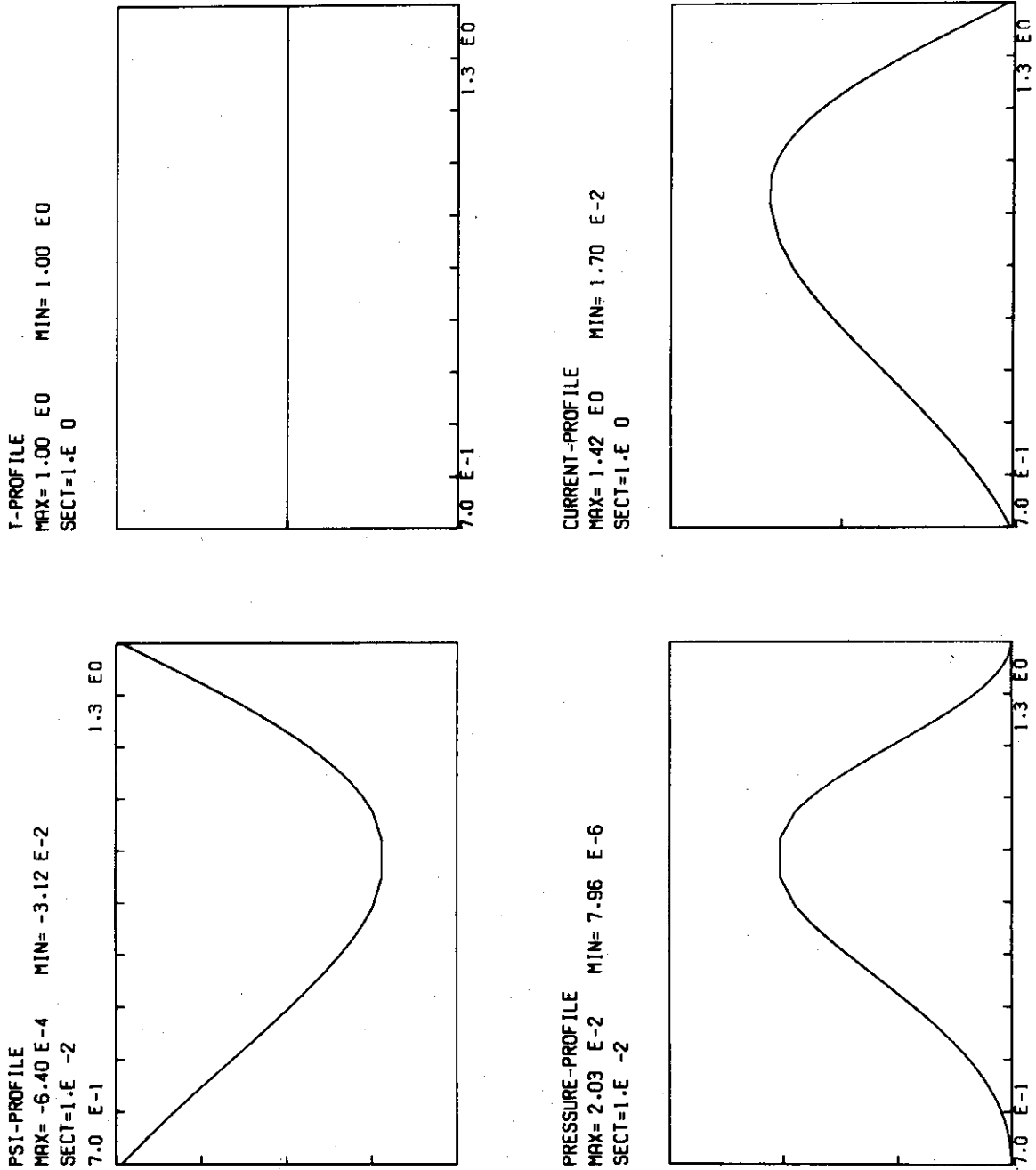


Fig. 8 (c-2)

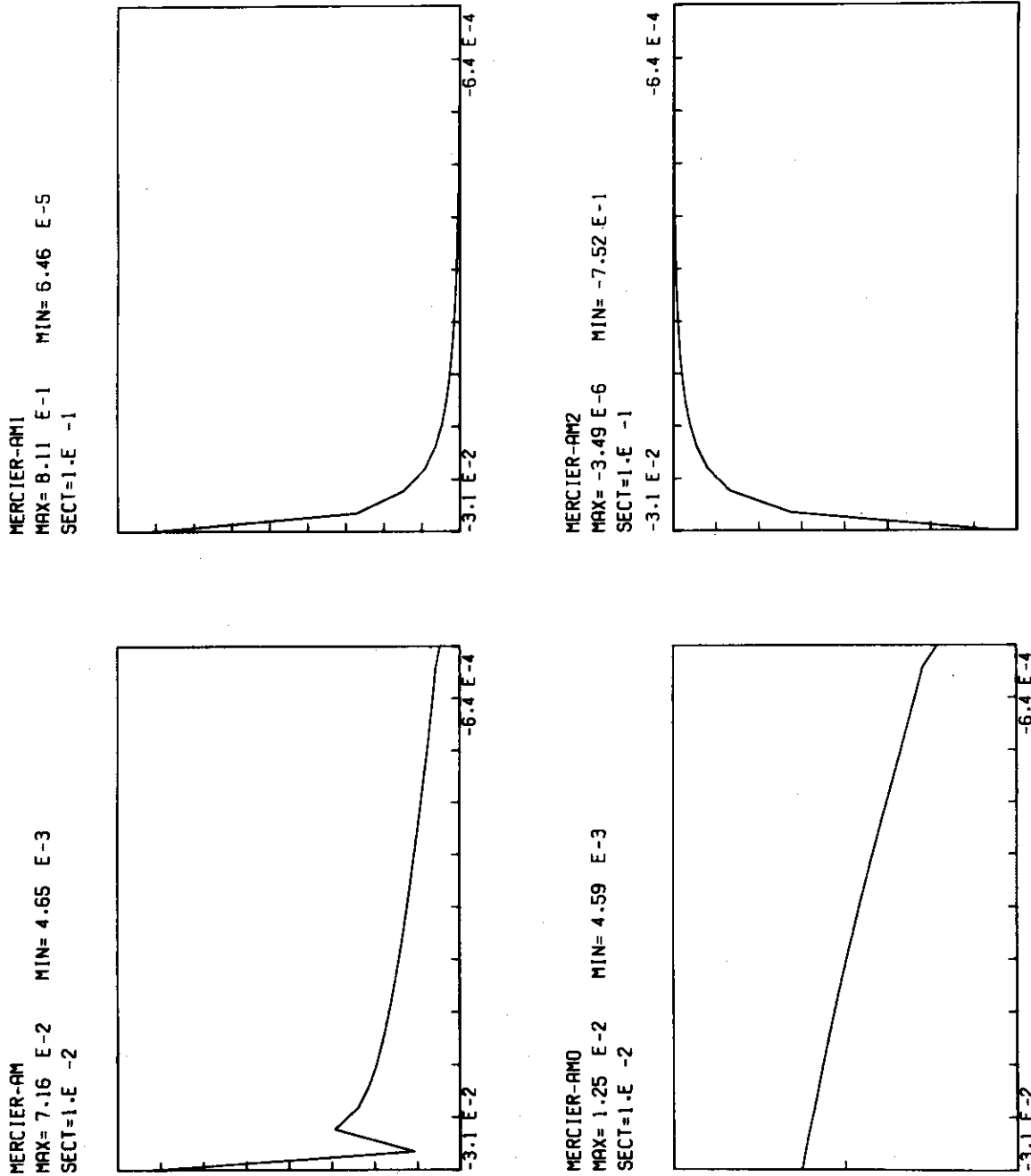


Fig. 8 (c-3)

# PARAMETERS

ISIGMA= 5

ISTOT= 3

QC= 1.28

SIGMA= 0.0340

BETA= 0.0105

BETAP= 0.895

BETAST= 0.0159

Q-PROFILE  
 MAX= 4.80 E0    MIN= 1.28 E0  
 SECT=1.E 0

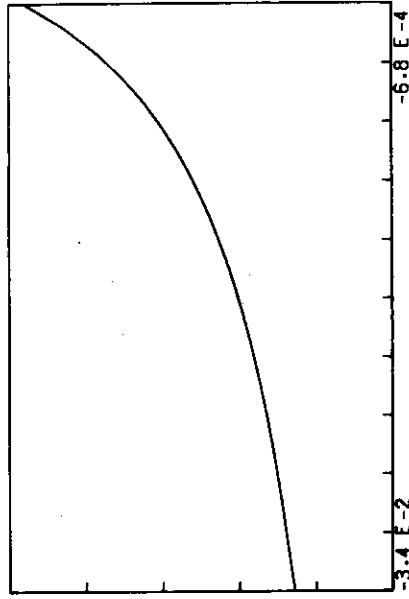


Fig.8 Examples of results for different values of scaling factor  $\sigma$ .

(d)  $\sigma=0.034$

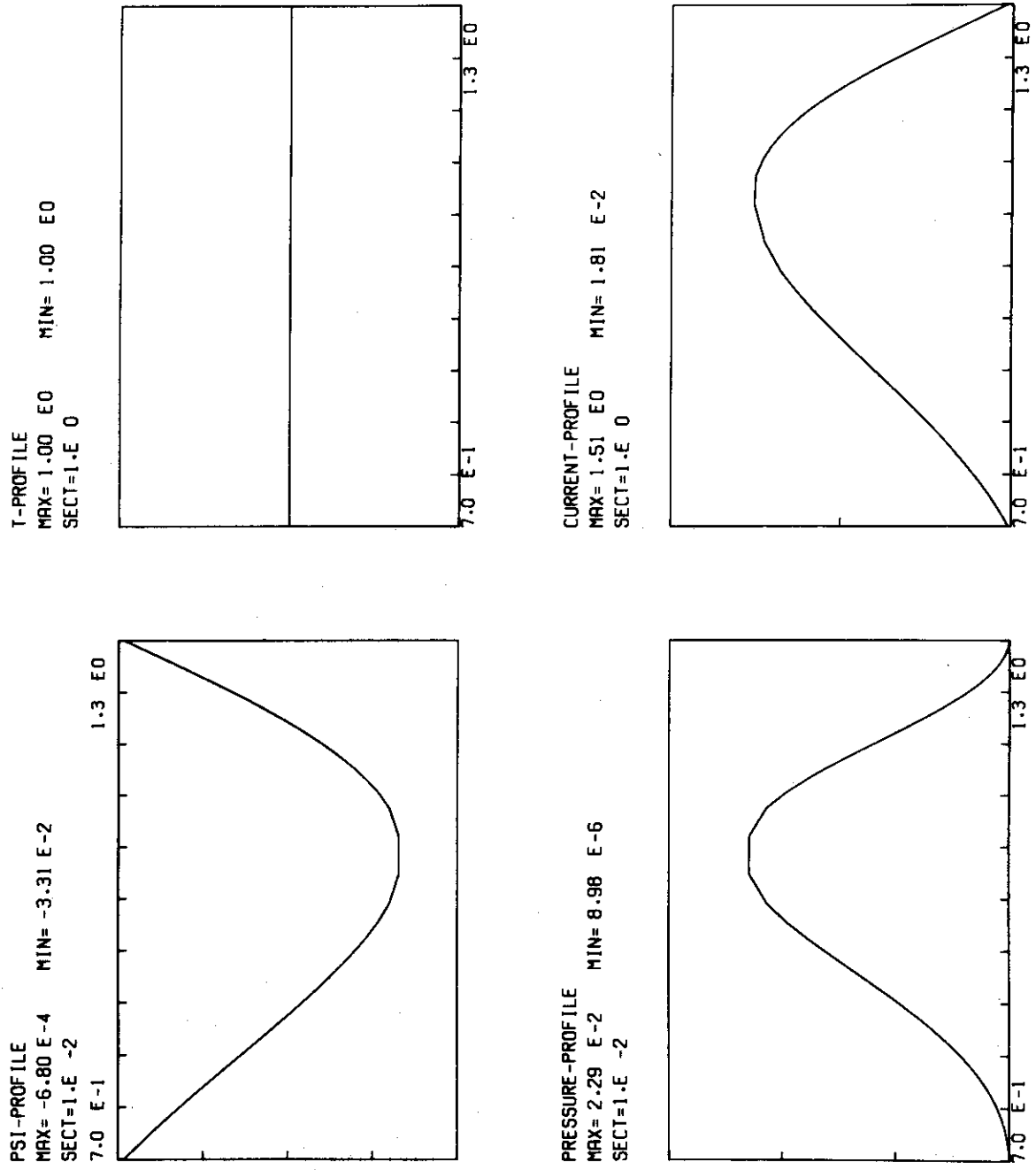


Fig. 8 (d-2)



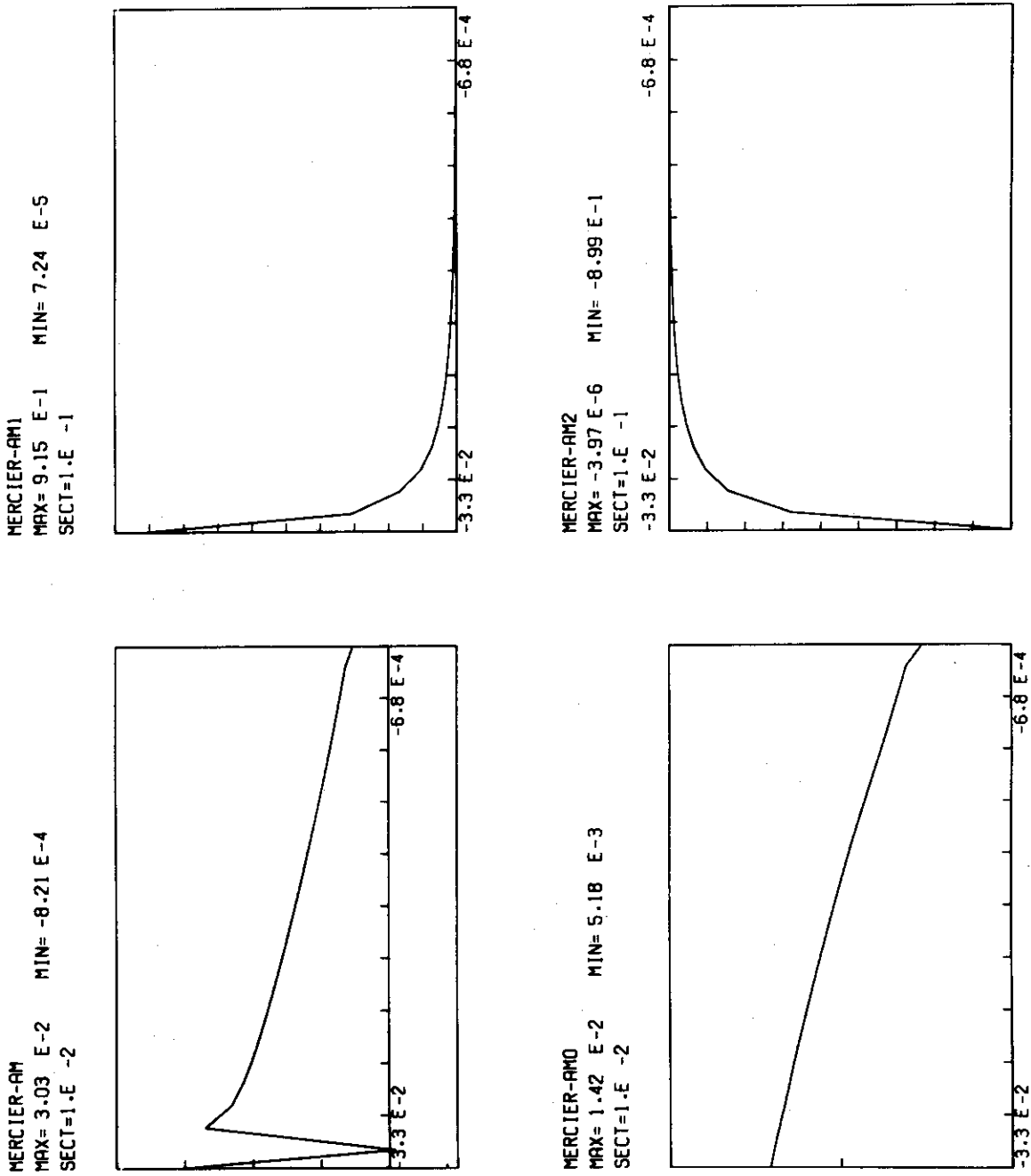


Fig. 8 (d-3)

# PARAMETERS

ISIGMA= 5  
 ISTOT= 4  
 QC= 1.21  
 SIGMA= 0.0360  
 BETA= 0.0117  
 BETAP= 0.895  
 BETAST= 0.0178

Q-PROFILE  
 MAX= 4.53 E0    MIN= 1.21 E0  
 SECT=1.E 0

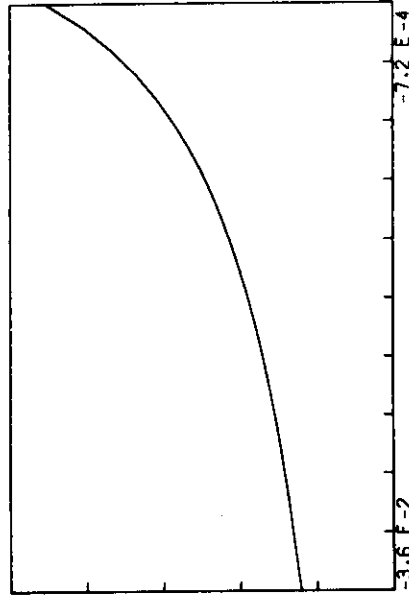


Fig.8 Examples of results for different values of scaling factor  $\sigma$ .

(e)  $\sigma=0.036$

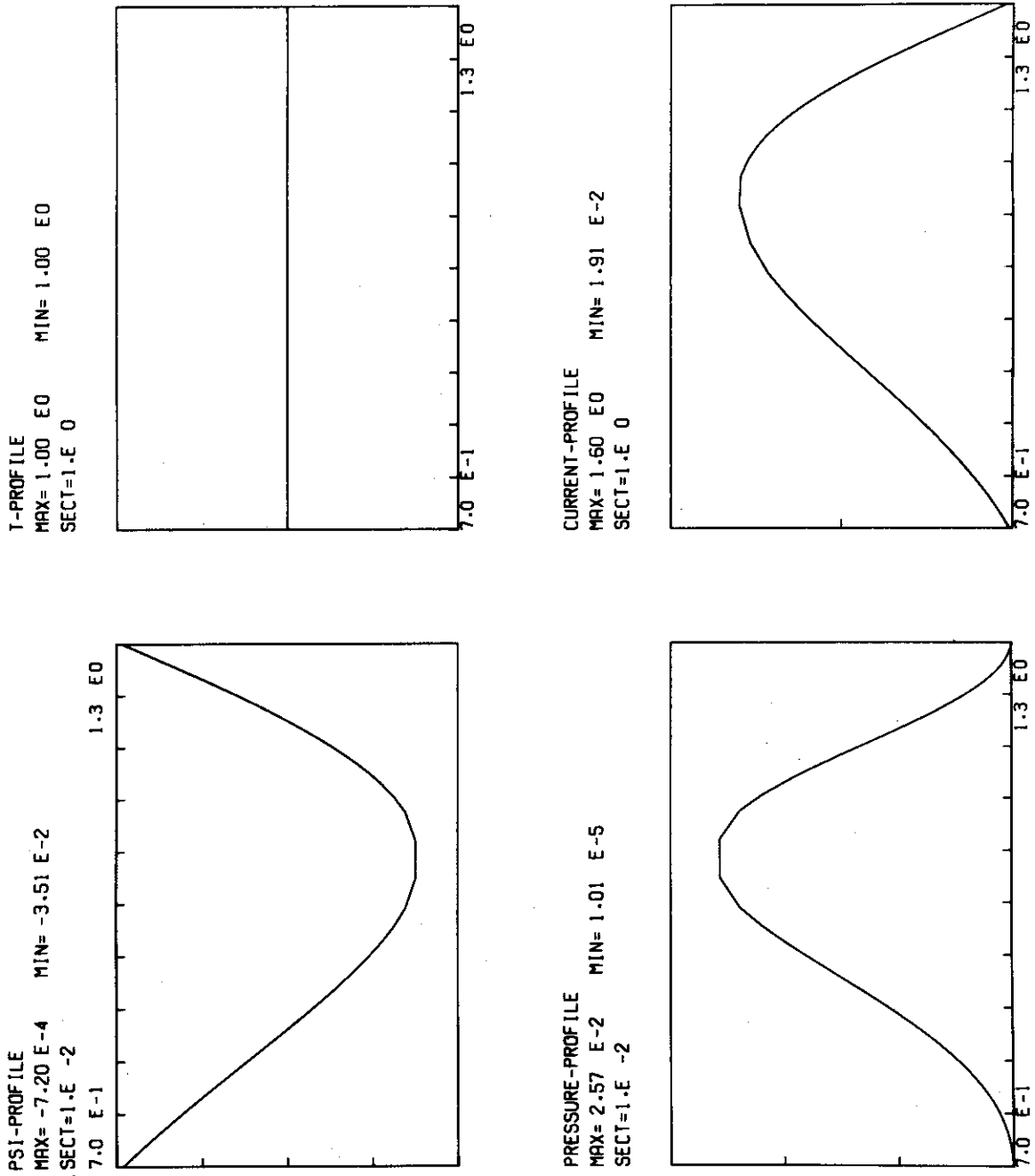


Fig. 8 (e-2)

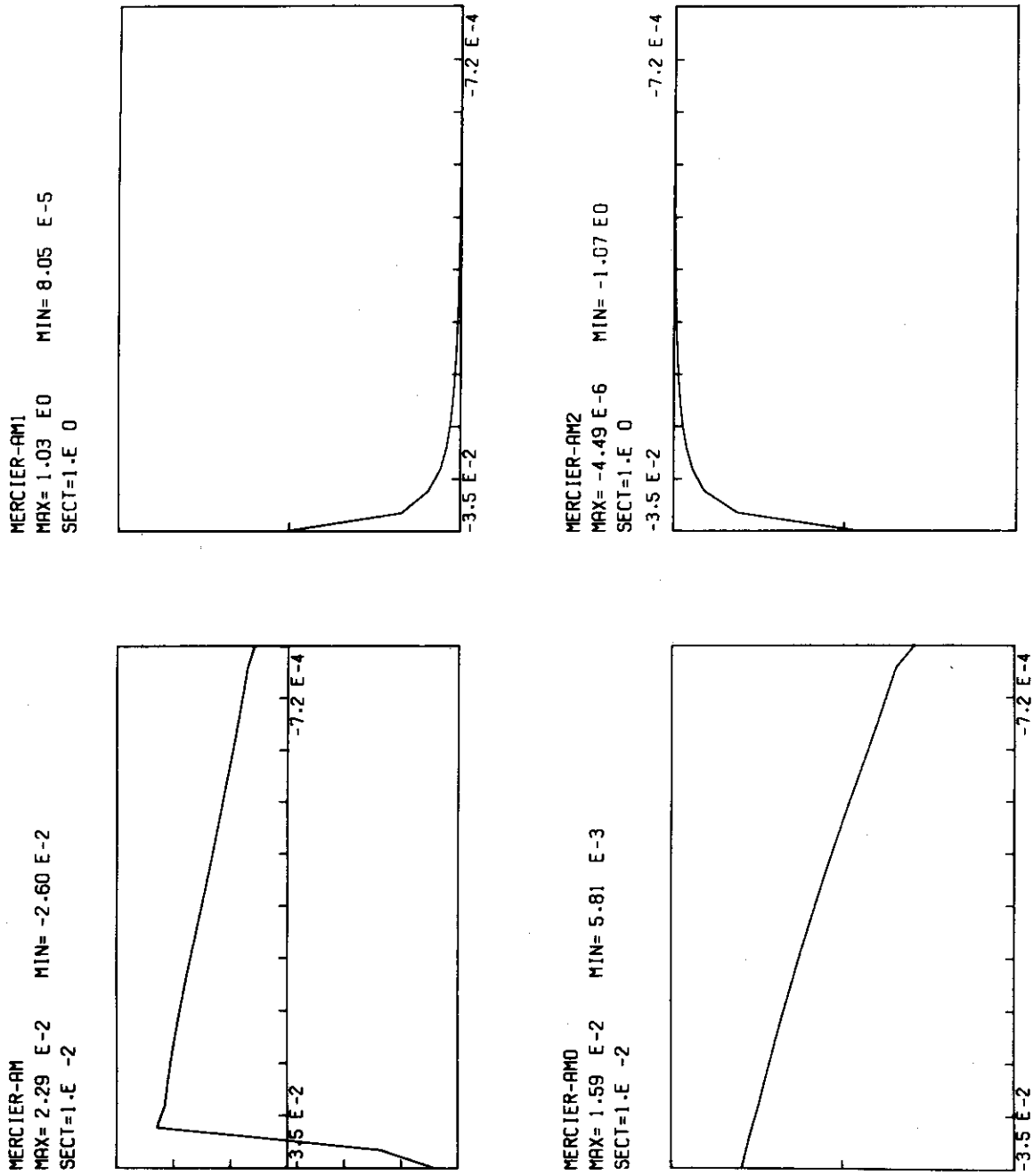


Fig. 8 (e-3)

APPENDICES



A1.2 COMMON variables

COMMON BLOCKS (INTEGER)

Label of COMMON BLOCKS	I C M S I Z	I C M O U T	I C M N O D	I C M M S H	I C M F I L	I C M I T R	I C M K N D	I C M O P T	I C M B N D	I C M S C L
MAIN	0									
ABCDCL		0								
BTYPE		0	0	0	0					
CDEYTP		0		0	0					
CENELM										
CNTMSH				0						
CNTSTR		0	0	0						
CORDXY		0	0	0		0	0			
DIFF										
ELMSCH			0	0						
FUNC										
FUNCF1										
INLOOP			0	0	0	0	0			
INPUT		0		0	0			0	0	0
INTGRL										
INTMSH		0	0	0		0		0		
ITERAT				0		0				
LINEQ										
LINTP										
MAGAXS			0	0						
MATELM										
MATGEN		0	0	0		0	0			
MERCIR				0						
NUMBER		0	0	0			0			
OLDNEW			0							
OUTPUT	0	0	0	0	0					0

COMMON BLOCKS (REAL)

Label of COMMON BLOCKS	R	R	R	R	R	R	R	R	R	R	R	R	R	R	R	R
Name of SUBROUTINES	C	C	C	C	C	C	C	C	C	C	C	C	C	C	C	C
	M	M	M	M	M	M	M	M	M	M	M	M	M	M	M	M
	A	C	S	G	C	P	B	T	V	M	L	B	T	P	L	M
	B	O	C	S	D	Q	E	L	U	S	N	N	H	L	N	E
	C	R	L	S	E	T	T	T	P	H	G	D	E	A	G	R

MAIN																
ABCDCL	O															
BTYPE		O	O	O												
CDETP			O	O	O	O	O	O	O							
CENELM	O															
CNTMSH																
CNTSTR		O								O						
CORDXY		O		O							O	O	O			
DIFF																
ELMSCH		O														
FUNC	O			O												
FUNCF1			O	O										O		
INLOOP		O		O						O						
INPUT			O	O						O		O		O	O	
INTGRL																
INTMSH		O		O						O		O	O		O	
ITERAT				O						O						
LINTP																
MAGAXS		O		O												
MATELM	O															
MATGEN		O														
MERCIR					O	O		O								O
NUMBER																
OLDNEW		O														
OUTPUT		O	O	O	O		O	O				O		O		O



COMMON variables

## \*Integer

/ICMSIZ/ Memory size  
 MATSIZ,IVECSZ,NODSIZ,NELMSZ  
 /ICMFIL/ File data  
 NFOUT,NFEQU,NFST1,NFST2,NFST3  
 /ICMNOD/ F.E.M. data  
 NODELM(1650,4),NODBOD(150),NODSYM(200),  
 MAXNOD,MAXELM,MAXBOD,MAXSYM,MAXVAR  
 /ICMMSH/ F.E.M. and iteration data  
 NDIV,NDIV1,MDIV,MDIV1,IDPS(100),  
 ITRMXI,ITRMXO,ICHNGO  
 /ICMKND/ F.E.M. data  
 NODKND(1700),IDIF  
 /ICMBND/ F.E.M. data (boundary shape)  
 ISHAPE,NPNT  
 /ICMITR/ Iteration data  
 ITRIN,ITROUT  
 /ICMSCL/ Scaling data  
 ISIGMA,ISTOT  
 /ICMOUT/ Output control  
 IOUT(20)  
 /ICMOPT/ Option data  
 ITITLE(18),IOPT(20)

## \*Real

/RCMABC/ F.E.M. data  
 A3(3),B3(3),C3(3),A4(4),B4(4),C4(4),D4(4)  
 /RCMLNG/ F.E.M. data  
 RDLN(101)  
 /RCMTHE/ F.E.M. data  
 DCOSTT(250)  
 /RCMBND/ F.E.M. data (boundary shape)  
 RC,ASP,ELL,DLT, RBND(250), ZBND(250)

/RCMESH/ F.E.M. and iteration data  
PLYR(100),EPSINM,EPSOUM,EPSIN,EPSOU

/RCMGSS/ Iteration data  
ALAM,DAXIS,PSMX,AXOLD

/RCMPLA/ Plasma data  
PPARA(10),TPARA(10)

/RCMCOR/ Mesh data  
PASN(1700),PCAL(1700),ROLD(1700),ZOLD(1700),  
RNEW(1700),ZNEW(1700),RBOD(150),ZBOD(150),  
RTMP(150),ZTMP(150)

/RCMPQT/ Solution  
OPS(100),OT(100),OPR(100)

/RCMSCL/ Scaling factor  
SIGMA,DSIGMA

/RCMCDE/ Surface quantities and volume integrals  
OCHI(1700),OQ(100),OC1(100),OC2(100),OC3(100),  
OC4(100),OC5(100),OIP,OIP2,OIB2,OIV,OII,OC

/RCMVUP/ Surface quantities  
VPR(100),UPR(100),VPP(100),UPP(100),SSS(100)

/RCMBET/ Beta values  
BETA,BETAP,BETAST

/RCMMER/ Mercier criterion  
AM(100),AM0(100),AM1(100),AM2(100)

/RCMPLT/ Data for plotting  
PSPLT(200),PRPLT(200),TPPLT(200),  
CUPLT(200),RRPLT(200)

## A2. Job control statement

```

1   *NO RSEL1,0205 , P.0C.3T.5W.2, C35
2   *USER J2636 ,
3   VM *GJOB 3112636,TA,TAKEDA,021.12,SMF=CLS
4   VM *LIBE,L J2636,SELDATA,((SEL10D40)),SYSOUT=CLS
5   VM *HFORT J2636,SELENE10,SYSOUT=CLS
6   VM *HLIEDRUN SYSOUT=CLS
7   *FD READ,FILE=(CATLG,J2636,SELDATA(SEL10D40))
8   VM *TPDISK F77
9   VM *TPDISK F90
10  VM *TPDISK F91
11  VM *TPDISK F92
12  VM *TPDISK F93
13  VM *HRUN EFNAME=J2636,GRAPHEBB,NAME=2,SYSOUT=CLS
14  VM *GCOM35
15  VM *TPDISK F77
16  *JEND

```

## \* remarks

```

J2636.SELDATA.....Input data file
J2636.SELENE10.....Source program file
J2636.GRAPHEBB.....EB file of a graphic output program

```



```

DLT=0.0
DO 500 I=1,250
  RBND(I)=0.0
  ZBND(I)=0.0
500 CONTINUE
  IDPSO=0
  DO 600 I=1,100
    IDPSN=I**2
    IDPS(I)=IDPSN-IDPSO
    IDLN(I)=1
    IDPSO=IDPSN
600 CONTINUE
  DO 700 I=1,20
    IOUT(I)=0
700 CONTINUE
  NFOUT=77
  NFEQU=90
  NFST1=91
  NFST2=92
  NFST3=93
  ICHNGO=3
  ITRMXI=10
  ITRMXO=5
  EPSINM=1.0D-6
  EPSOUM=1.0D-8
  ISIGMA=1
  ISTOT =0
  ALAM=1.0
  DAXIS=0.0
  PSMX=1.0
  SIGMA=0.01
  DSIGMA=0.01
C
C
C
  READ (5,INOPT)
  READ (5,RNPLA1)
  READ (5,RNPLA2)
  READ (5,INBND)
  IF (ISHAPE,GE,3) GO TO 1100
  READ (5,RNBND1)
  GO TO 1200
1100 READ (5,RNBND2)
  READ (5,RNBND3)
1200 READ (5,INMSH1)
  READ (5,INMSH2)
  READ (5,INMSH3)
  READ (5,INMSH4)
  READ (5,RNMSH1)
  READ (5,RNGSS)
  READ (5,INDUT)
  NDIV=NDIV+1
  MDIV=MDIV+1
  DLTOT=0.0
  DO 2000 J=1,NDIV
    DLTOT=DLTOT+DLN(J)
2000 CONTINUE
  RDLN(I)=0.0
  DO 2100 J=2,NDIV1
    RDLN(J)=RDLN(J-1)+DLN(J)/DLTOT
2100 CONTINUE
  IF (DAXIS.LE,0.0) DAXIS=RC
C
C
C
  ** WRITE INPUT DATA **
  WRITE(6,6000) (ITITLE(I),I=1,18)
6000 FORMAT(1H1///1H ,10X,7Z(1H#)///1H ,10X,18A4//
1 1H ,10X,7Z(1H#)///)
C
C
C
  WRITE(6,6001) (IOPT(I),I=1,20)
  WRITE(6,6002) (PPARA(I),I=1,10)
  WRITE(6,6003) (TPARA(I),I=1,10)
  WRITE(6,6004) (ISHAPE, NPNT)
  WRITE(6,6005) RC, ASP, ELL, DLT
  WRITE(6,6006) (RBND(I),I=1, NPNT)
  WRITE(6,6007) (ZBND(I),I=1, NPNT)
  WRITE(6,6008) NDIV, MDIV
  WRITE(6,6009) (IDPS(I),I=1, NDIV)
  WRITE(6,6010) (IDLN(I),I=1, NDIV)
  WRITE(6,6011) ITRMXI, ITRMXO, ICHNGO, ISIGMA
  WRITE(6,6012) EPSINM, EPSOUM
  WRITE(6,6013) ALAM, DAXIS, PSMX
  WRITE(6,6014) (IOUT(I),I=1, 20)
  WRITE(6,6015) SIGMA, DSIGMA
C
C
C
  ** OUTPUT FORMAT **
6001 FORMAT(1H0,4X,'IOPT=',20I5)
6002 FORMAT(1H0,4X,'PPARA=',10E12,5)
6003 FORMAT(1H0,4X,'TPARA=',10E12,5)
6004 FORMAT(1H0,4X,'ISHAPE=',13,2X,'NPNT=',13)
6005 FORMAT(1H0,4X,'RC=',E12,5,2X,'ASP=',E12,5,2X,'ELL=',E12,5,2X,
1 'DLT=',E12,5
2 )
6006 FORMAT(1H0,4X,'RBND=',10E12,5/(10X,10E12,5))
6007 FORMAT(1H0,4X,'ZBND=',10E12,5/(10X,10E12,5))
6008 FORMAT(1H0,4X,'NDIV=',15,2X,'MDIV=',15)
6009 FORMAT(1H0,4X,'IDPS=',20I5/(10X,20I5))
6011 FORMAT(1H0,4X,'ITRMX(INLOOP) =',15,2X,
1 'ITRMX(OUTLOOP) =',15,2X,'ICHNGO =',15,2X,'ISIGMA =',15)
6013 FORMAT(1H0,4X,'EPSINM =',E12,5,2X,'EPSOUM =',E12,5)
6014 FORMAT(1H0,4X,'ALAM =',E12,5,2X,'DAXIS =',E12,5,2X,'PSMX =',E12,5)
6015 FORMAT(1H0,4X,'IOUT =',20I5)
6016 FORMAT(1H0,4X,'IDLN =',20I5/(10X,20I5))
6017 FORMAT(1H0,4X,'SIGMA =',E12,5,2X,'DSIGMA =',E12,5)
C
C
  RETURN
  END

```

INP11500  
INP11600  
INP11700  
INP11800  
INP11900  
INP12000  
INP12100  
INP12200  
INP12300  
INP12400  
INP12500  
INP12600  
INP12700  
INP12800  
INP12900  
INP13000  
INP13100  
INP13200  
INP13300  
INP13400  
INP13500  
INP13600  
INP13700  
INP13800  
INP13900  
INP14000  
INP14100  
INP14200  
INP14300  
INP14400  
INP14500  
INP14600  
INP14700  
INP14800  
INP14900  
INP15000  
INP15100  
INP15200  
INP15300  
INP15400  
INP15500  
INP15600  
INP15700  
INP15800  
INP15900  
INP16000  
INP16100  
INP16200  
INP16300  
INP16400  
INP16500  
INP16600  
INP16700  
INP16800  
INP16900  
INP17000  
INP17100  
INP17200  
INP17300  
INP17400  
INP17500  
INP17600  
INP17700  
INP17800  
INP17900  
INP18000  
INP18100  
INP18200  
INP18300  
INP18400  
INP18500  
INP18600  
INP18700  
INP18800  
INP18900  
INP19000  
INP19100  
INP19200  
INP19300  
INP19400  
INP19500  
INP19600  
INP19700  
INP19800  
INP19900  
INP20000  
INP20100  
INP20200  
INP20300  
INP20400  
INP20500  
INP20600  
INP20700  
INP20800  
INP20900  
INP21000  
INP21100  
INP21200  
INP21300  
INP21400  
INP21500  
INP21600  
INP21700  
INP21800  
INP21900  
INP22000  
INP22100  
INP22200  
INP22300  
INP22400  
INP22500  
INP22600

## A3.2 An example of an input data set

```
TEST CALCULATION, DORY-TYPE
*INOPT *END
*RNPLA1 PPARA=1,50,0,7,4,0 *END
*RNPLA2 *END
*INBND ISHAPE=2 *END
*RNBND1 RC=1,,ASP=3,3,ELL=1,7,DLT=0,0 *END
*INMSH1 NDIV=30,MDIV=30 *END
*INMSH2 IDPS=40*1, *END
*INMSH3 ITRMXI=8,ITRMXO=5,ICHNGO=3 *END
*INMSH4 IDLN=40*1, *END
*RNMSH1 EPSINM=1,0D-5,EPSOUM=1,0D-5 *END
*RNGSS SIGMA=0,04 *END
*INOUT *END
```



M0	M1	M2	M
0.10345D-01	0.32072D-01	-0.36353D+01	-0.41796D+00
0.12071D-01	0.11099D+01	-0.12311D+01	-0.10914D+00
0.14293D-01	0.61665D+00	-0.57482D+00	0.56121D-01
0.15188D-01	0.40076D+00	-0.36716D+00	0.48788D-01
0.15076D-01	0.29163D+00	-0.26279D+00	0.43943D-01
0.15008D-01	0.22588D+00	-0.18984D+00	0.41046D-01
0.14959D-01	0.18184D+00	-0.15782D+00	0.38971D-01
0.14911D-01	0.15028D+00	-0.12786D+00	0.37340D-01
0.14884D-01	0.12659D+00	-0.10547D+00	0.36001D-01
0.14874D-01	0.10815D+00	-0.88155D-01	0.34870D-01
0.14884D-01	0.93387D-01	-0.74392D-01	0.33880D-01
0.14916D-01	0.81283D-01	-0.63206D-01	0.32990D-01
0.14989D-01	0.71168D-01	-0.53953D-01	0.32114D-01
0.15046D-01	0.62573D-01	-0.46176D-01	0.31442D-01
0.15144D-01	0.55136D-01	-0.39553D-01	0.30747D-01
0.15265D-01	0.48671D-01	-0.33849D-01	0.30087D-01
0.15411D-01	0.42933D-01	-0.28889D-01	0.29457D-01
0.15579D-01	0.37804D-01	-0.24538D-01	0.28844D-01
0.15769D-01	0.33165D-01	-0.20697D-01	0.28236D-01
0.15977D-01	0.28934D-01	-0.17288D-01	0.27623D-01
0.16201D-01	0.25048D-01	-0.14251D-01	0.26998D-01
0.16444D-01	0.21462D-01	-0.11545D-01	0.26361D-01
0.16704D-01	0.18135D-01	-0.91382D-02	0.25701D-01
0.16979D-01	0.15036D-01	-0.70093D-02	0.25006D-01
0.17265D-01	0.12148D-01	-0.51472D-02	0.24265D-01
0.17546D-01	0.94602D-02	-0.35493D-02	0.23476D-01
0.17895D-01	0.69727D-02	-0.22215D-02	0.22646D-01
0.18286D-01	0.46918D-02	-0.11781D-02	0.21799D-01
0.18820D-01	0.26270D-02	-0.44275D-03	0.21005D-01
0.17336D-01	0.61760D-03	-0.57124D-04	0.18096D-01

```

** MATRIX SIZE **
MATSIZ= 28800( 30000) MAXVAR= 900( 1700)
MAXNOD= 931( 1700) MAXELM= 900( 1650)
NFOUT= 77
NFEQ= 90
NFST1= 91
NFST2= 92
NFST3= 93
    
```